©2004 by Economic Geology
Vol. 99, pp. 1665–1686

Geochronology of the Midas Low-Sulfidation Epithermal Gold-Silver Deposit, Elko County, Nevada

E. D. Leavitt,†

Department of Geological Sciences, Mail Stop 172, University of Nevada, Reno, Reno, Nevada 89557-0001

T. L. Spell,

Department of Geoscience, University of Nevada, Las Vegas, 4505 Maryland Parkway, Las Vegas, Nevada 89154-4010

P. M. Goldstrand,

Bureau of Mining Regulation and Reclamation, 333 W. Nye Lane, Carson City, Nevada 98706

and G. B. Arehart

Department of Geological Sciences, Mail Stop 172, University of Nevada, Reno, Reno, NV 89557-0001

Abstract

The Midas deposit is the largest known high-grade Au-Ag vein deposit located along the northern Nevada rift. It belongs to a suite of middle Miocene low-sulfidation epithermal systems associated with magmatism and faulting along the rift. Interpretation of new $^{40}Ar/^{39}Ar$ dates for volcanic rocks and hydrothermal minerals related to gold mineralization and additional isotopic dates throughout the Midas region constrain the timing of volcanic, tectonic, and hydrothermal activity. The Midas hydrothermal system developed following a change from mafic-dominated bimodal volcanism and basin formation to felsic volcanism, folding, and faulting at about 15.6 Ma. From 15.6 to 15.2 Ma, sediments and tuffs were deposited on a relatively impermeable rhyolite flow. During this period, faulting and tilting of the volcanic edifice created pathways for hydrothermal fluids that flowed to the surface forming sinters and hydrothermal breccias. Approximately 200 kyr after the change in volcano-tectonic regime, oblique-slip faulting took place along zones of preexisting weakness, creating dilational zones and additional channelways for mineralizing fluids. At 15.4 Ma, high-grade veins formed in fault zones throughout the region, depositing at least 4 million ounces (Moz) of gold and 40 Moz of silver. The timing of high-grade Au-Ag mineralization is identical to the age of rhyolite intrusions whose source magma chamber likely provided the heat necessary to drive the hydrothermal system. The age of an unaltered tuff that unconformably overlies opalized sediments establishes that tilting of the units and the hydrothermal system had ceased by 15.2 Ma. The temporal and spatial coincidence of rhyolite volcanism, faulting, and high-grade mineralization may reflect the importance of contributions from deeper fluid reservoirs containing magmatic components or highly exchanged meteoric waters.

Introduction

The Ken Snyder mine exploits the largest known Au-Ag epithermal deposit along the middle Miocene northern Nevada rift. Located in the historic mining district of Midas, previously known as the Gold Circle district (LaPointe et al., 1991; Fig. 1), the deposit consists of a complex of steeply dipping, quartz-adularia-calcite-precious metal bonanza veins hosted by volcanic rocks. The Ken Snyder deposit, known worldwide as Midas, locally contains ore grades greater than 100 oz/t or 3,430 g/t of gold. Gold occurs as electrum and is intimately associated with selenide and sulfide minerals. Together, these minerals form dark bands similar to the ginguro ore at Hishikari (e.g., Izawa et al., 1990; Naito, 1993). Premining reserves at Midas were approximately 3 Moz of Au and 35 Moz of Ag (0.25 oz/t or 8.5 g/t Au cutoff grade; R. Streiff, pers. commun., 2003), with the bulk of the ore contained within the Colorado Grande and Gold Crown veins. Exploration efforts in the district are ongoing, and potential resources remain untested.

† Corresponding author: e-mail, zoracdavie@aol.com

Midas is a selenide-rich, low-sulfidation, epithermal system, and it belongs to a suite of precious metal occurrences that formed along the northern Nevada rift between 15.6 and 15.0 Ma (John, 2001; Fig. 1). These low-sulfidation systems have been referred to as Au-rich end-member low-sulfidation systems by Hedenquist et al. (2000) or type 2 epithermal systems by Albino and Margolis (1991), John et al. (1999), and John (2001). They formed from fluids dominated by meteoric water of near-neutral pH and have relatively high Au/Ag ratios, low total base metal contents, high selenide mineral contents, and predominantly reduced sulfur (John et al., 1999, 2003; John and Wallace, 2000; John, 2001). They are most commonly associated with rhyolite flows and domes in extensional rift environments (John, 2001), although along the northern Nevada rift examples of both mafic- and felsic-hosted systems exist (John, 2001). Similar temporal associations between low-sulfidation epithermal systems, magmatism, and faulting have been observed in rift-related, continental extension, and/or backarc settings elsewhere in the world (Sillitoe and Hedenquist, 2003).

Midas formed during a middle Miocene pulse of bimodal basalt-rhyolite magmatism that was widespread throughout

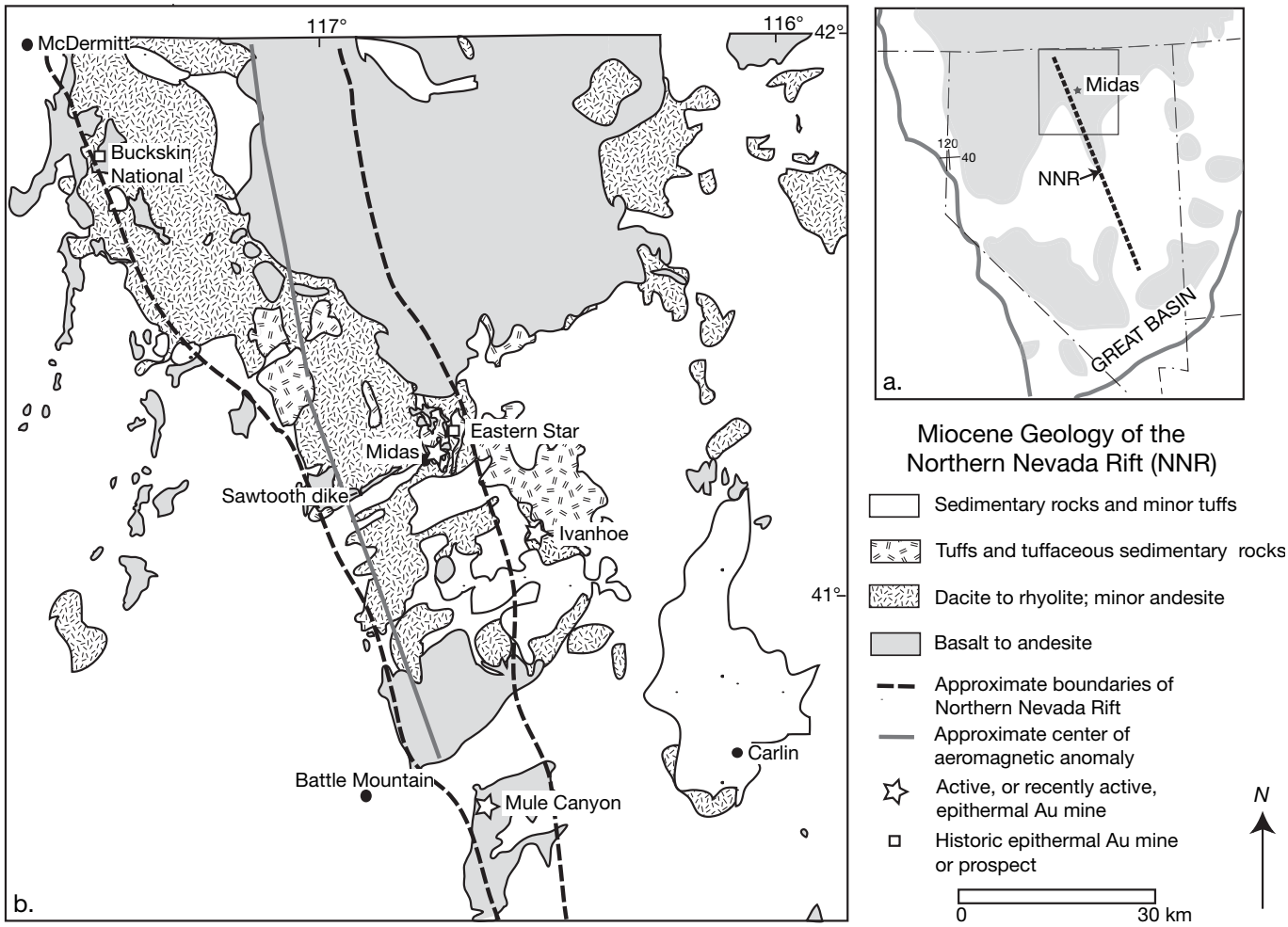

FIG. 1. Location and general geology of the northern Nevada rift. a. Bimodal basalt-rhyolite assemblage (shaded) and axis of northern Nevada rift. Modified from Christiansen and Yeats (1992), Ludington et al. (1996), and John (2001). b. Approximate locations of volcanic-hosted, low-sulfidation epithermal precious metal occurrences associated with the northern Nevada rift. Modified from Stewart and Carlson (1976) and John and Wallace (2000).

the northern Great Basin (Christiansen and Yeats, 1992; Fig. 1). The temporal and spatial association between epithermal systems and volcanic activity led some workers to propose that mafic volcanism was a source of gold and other components of these epithermal systems, i.e., there was a magmatic contribution to the ore-forming systems from coeval mafic magmatism (Noble et al., 1988; Connors et al., 1993; John, 2001; John et al., 2003). Other workers noted the possibility of a genetic connection between rhyolites and low-sulfidation Au-Ag mineralization (Bonham, 1988). However, although spatially and temporally related, a direct genetic relationship between magmatism and most meteoric water-dominated low-sulfidation systems along the rift, or elsewhere in the northern Great Basin, has not been demonstrated (John, 2001).

Understanding the temporal relationship between low-sulfidation epithermal precious metal systems and their volcanotectonic settings continues to evolve. In the 1980s, a limited number of geochronologic studies of low-sulfidation systems resulted in a model that invoked a temporal gap of greater than 1.0 m.y. between formation of volcanic host rocks and mineralization; therefore, a genetic relationship was deemed unlikely (e.g., Heald et al., 1987). However, in detail, studies of some low-sulfidation systems did not support this. A geologic and K-Ar geochronologic study of the National district (Fig. 1), approximately 80 km northwest of Midas, located within a middle Miocene bimodal volcanic assemblage along the western margin of the northern Nevada rift, indicated that formation of precious metal veins was coeval with eruption of an altered, mineralized rhyolite (Vikre, 1985). Other, more recent geochronologic studies of middle Miocene, low-sulfidation systems that have employed more precise $^{40}Ar/^{39}Ar$ dating methods document shorter time gaps (≤500 kyr) between the formation of volcanic host rocks and mineralization, such as at Round Mountain in central Nevada (Henry et al., 1997) and Sleeper in northwestern Nevada (Conrad and McKee, 1996). Although the gap between the age of volcanic host rocks and the age of ore appears to be narrowing, coeval formation of host rocks and ore has not been demonstrated, and links to magmatism are difficult to prove.

Several K-Ar dates on surrounding volcanic rocks and mineralized veinlets within the Midas district and results of this study have shown that the age of Midas is similar to that of other epithermal occurrences along the rift (McKee et al., 1976; Wallace et al., 1990; Wallace, 1993; Wallace and McKee, 1994; Leavitt et al., 2000, 2003; Leavitt, 2001). Only a few geochronologic studies of this group of deposits have been carried out using $^{40}Ar/^{39}Ar$ methods (John et al., 2003; Wallace, 2003), and prior to this study, no $^{40}Ar/^{39}Ar$ dates had been determined for the high-grade veins, host rocks, or surrounding volcanic rocks at Midas. Preliminary results, including three new dates, were published in Leavitt et al. (2000). In this paper, we describe the complete data set on volcanic rocks and mineralization in the Midas area, including five additional dates. As the largest known ore deposit along the northern Nevada rift, Midas provides an excellent opportunity to document the temporal relationships between magmatism, extension, and low-sulfidation epithermal mineralization. Data from this study provide constraints on the timing and duration of the Midas hydrothermal system and regional volcano-tectonic events.

Regional Geologic Setting and Ore Deposits

Midas is located near the eastern margin of the northern Nevada rift. The northern Nevada rift is a geographic term for a lineament that extends from east-central Nevada to southern Oregon (Fig. 1a; Zoback and Thompson, 1978; Zoback et al., 1994; John and Wallace, 2000). The northern Nevada rift is defined by a positive aeromagnetic anomaly that locally corresponds to an alignment of middle Miocene eruptive centers including mafic dike swarms and intermediate to silicic intrusions and vents, fossil geothermal systems, and grabens (John and Wallace, 2000; John et al., 2000). The northern Nevada rift formed during Basin and Range extension (Zoback et al., 1994; John, 2001; Dickinson, 2002), and its location may have been controlled in part by preexisting zones of weakness (Theodore et al., 1998; John et al., 2000). Similar subparallel aeromagnetic anomalies within the northern Great Basin lie west of the northern Nevada rift (Blakley and Jachens, 1991; Glen and Ponce, 2002; Ponce and Glen, 2002). These lineaments are most likely due to the episode of extension that generated the northern Nevada rift; however, a correlation between the western anomalies with middle Miocene igneous rocks is unclear (Ponce and Glen, 2002).

The formation of Midas and other low-sulfidation epithermal systems was coeval with bimodal, basalt-rhyolite activity along the northern Nevada rift. Ages of volcanism along the rift range from approximately 16.5 to 14.7 Ma (Zoback et al., 1994; John and Wallace, 2000; John et al., 2000; Leavitt et al., 2000, 2003; Leavitt, 2001; Wallace, 2003). Mafic volcanic rocks are predominantly K-rich tholeiitic basalts, basaltic andesites, and andesites. The abundance of felsic rocks increases in the central and northern portions of the rift (Fig. 1b), as well as in the upper portion of the rift sequence. Faulting accompanied, and locally postdated, magmatism and hydrothermal activity along the rift (Wallace, 1993; John et al., 2000). Middle Miocene bimodal basalt-rhyolite igneous activity was coeval with deposition of a high K, calc-alkaline assemblage of igneous rocks of dominantly intermediate compositions during the waning stages of a continental arc to the west (western andesite assemblage of John et al., 1999; John, 2001).

Intermediate-sulfidation (Hedenquist et al., 2000; Sillitoe and Hedenquist, 2003) epithermal deposits (type 1 low-sulfidation of Albino and Margolis, 1991; John et al., 1999; John, 2001) that formed in the western andesite assemblage have been distinguished from low-sulfidation systems based on ore mineralogy and volcano-tectonic setting (John et al., 1999; John and Wallace, 2000; John, 2001). Compared to low-sulfidation systems, the intermediate-sulfidation systems contain more silver and total base metals and variable but low quantities of selenide minerals; isotopic evidence indicates the presence of magmatic fluids (e.g., Comstock Lode, Taylor, 1973; O'Neil and Silberman, 1974; Vikre, 1989; Simmons, 1995; John, 2001).

District Geology

The Midas deposit is hosted by a deeply eroded section of Miocene volcanic rocks along the eastern margin of the northern Nevada rift (Fig. 1b). The volcanic rocks of the district have been delineated and characterized by geologic mapping of the Snowstorm Mountains (Wallace, 1993), Midas district (Emmons, 1910; Rott, 1931; Blair, 1991), and the Ken Snyder mine (Casteel et al., 1999; Goldstrand and Schmidt, 2000), and petrographic work for this study. Drilling in the Midas area has shown that Miocene tuffs, flows, and volcaniclastic rocks extend to a depth of at least 1.5 km beneath the present surface. The depth to older Tertiary volcanic rocks as well as pre-Tertiary basement beneath Midas is unknown. The closest surface exposures of older Tertiary and Paleozoic rocks are approximately 10 km southeast of Midas. The Miocene bimodal basalt-rhyolite sequence includes felsic ash-flow and airfall tuffs, flows, plugs, tuffaceous lacustrine deposits, and mafic dikes, sills, and flows (Fig. 2). A geologic map and cross section of the Midas area compiled from sources described above and recent mapping by Newmont project geologists display the distribution of units (Figs. 3–4). As presently known, ore is confined to steeply dipping, banded quartz veins filling north-northwest–striking faults in felsic units (e.g., Colorado Grande and Gold Crown; Fig. 3). Unaltered rhyolite vitrophyre and ash-flow tuff overlie hydrothermally altered host rocks.

Miocene stratigraphy

The lower tuff unit (Tlt) forms the base of the altered section of Miocene ash-flow tuffs in the district (Goldstrand and Schmidt, 2000; Fig. 2). This unit consists of ≥775 m of brown-gray, crystal-lithic, weakly welded tuff. Sanidine and plagioclase are the dominant phenocrysts and form up to 10 vol percent of the tuff. Sanidine crystals are altered and exhibit mottled extinction typical of adularization (Henry et al., 1997). Lithic fragments include small rounded clasts of andesite, pumice, and quartz-bearing and welded tuffs.

The June Belle formation (informal, Tjb) overlies the lower tuff unit (Blair, 1991; Wallace, 1993; Goldstrand and Schmidt, 2000) and comprises a rhyolite flow-dome-tuff complex, 10 to 250 m thick. Flow foliation has gentle to vertical dips; near the Elko Prince mine, approximately 2 km north-northwest of the Ken Snyder mine (Fig. 3), vertical flow foliations and breccias along contacts are interpreted to

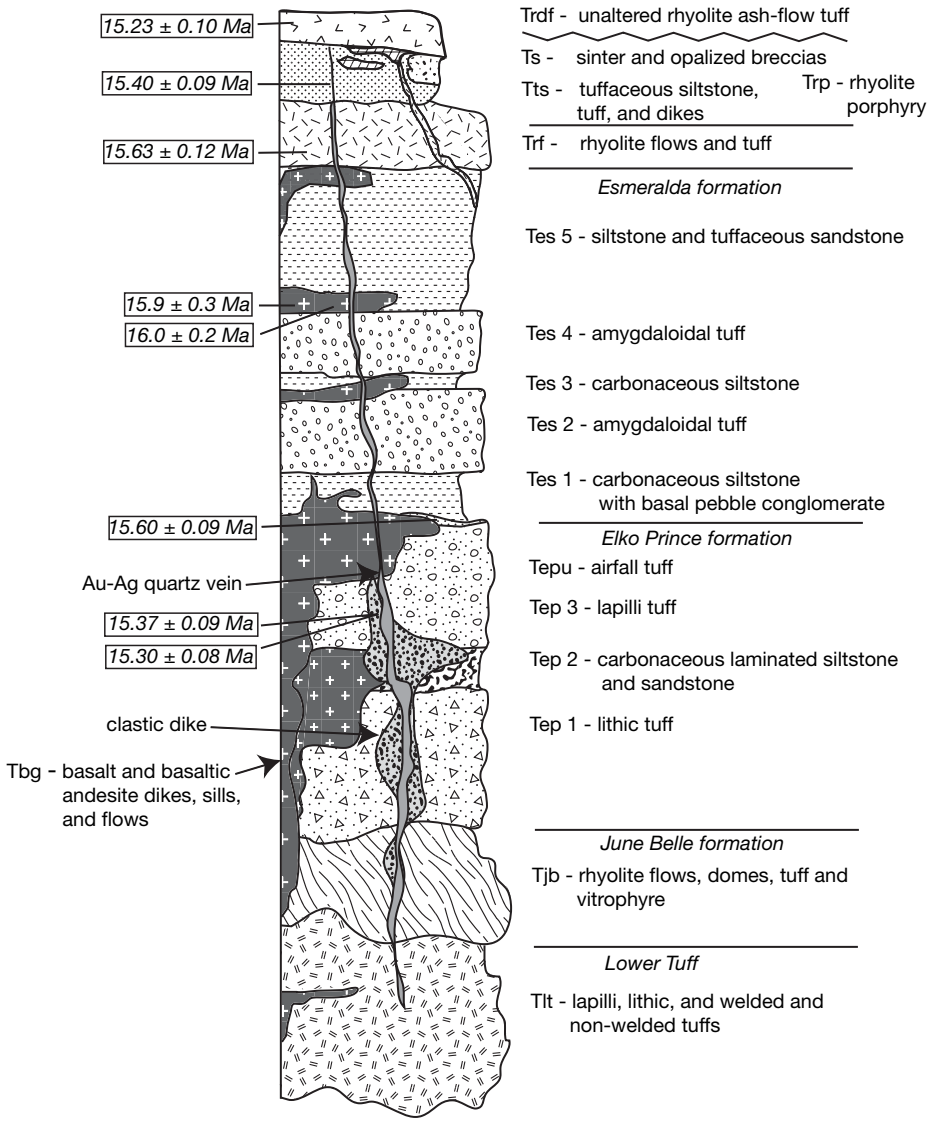

FIG. 2. Generalized stratigraphic section of the Midas deposit. Modified from Goldstrand and Schmidt (2000). Relative locations and ages of geochronology samples shown.

indicate the presence of a vent (Blair, 1991). Vitrophyric rocks are common at the bottom and top of the unit, and eutaxitic textures are present locally. Sanidine and plagioclase are the dominant phenocrysts and form up to 15 vol percent of rock. Lithic fragments include rounded clasts of andesite, basalt, and welded tuff. The mafic clasts reach 10 cm in size near the base of the unit. Sparse glass shards and continuous, locally vertical, banding suggest that this unit is composed primarily of flows and domes or rheomorphic tuffs (Henry and Wolff, 1992). Spherulitic devitrification is well-developed locally. As in the lower tuff unit, sanidine crystals are altered and exhibit mottled extinction.

The Elko Prince formation (informal, Tep) has both gradational and sharp contacts with the underlying June Belle formation. The Elko Prince formation is composed of a variety of ash-flow tuffs and volcaniclastic sedimentary rocks and has been divided into three informal members (Goldstrand and Schmidt, 2000; Fig. 2). The lower member (Tep 1) is up to 155 m thick and consists of green-gray poorly welded lithic-crystal ash-flow tuff that contains clasts of basalt, welded tuff, banded rhyolite, and pumice. An intermediate member (Tep 2), composed of gray carbonaceous lacustrine, volcaniclastic sedimentary rocks, is laterally discontinuous and up to 30 m thick. The presence of angular fragments and crystals and the distribution of this member suggest that these sediments are locally derived and accumulated in an aerially restricted basin (Goldstrand and Schmidt, 2000). The upper member (Tep 3) is composed of light-green lapilli tuff that has undergone little to no welding. A fine-grained, white, sanidine-rich air-fall tuff (Tepu) locally overlies Tep 3. Tep 3 grades upward into sediments of the Esmeralda formation (informal, Tes).

The Esmeralda formation (Tes), 85 to 260 m thick, consists of an alternating sequence of tuffaceous and carbonaceous lacustrine sedimentary rocks, pebble conglomerates, and fine-grained amygdaloidal tuffs that form five distinct informal

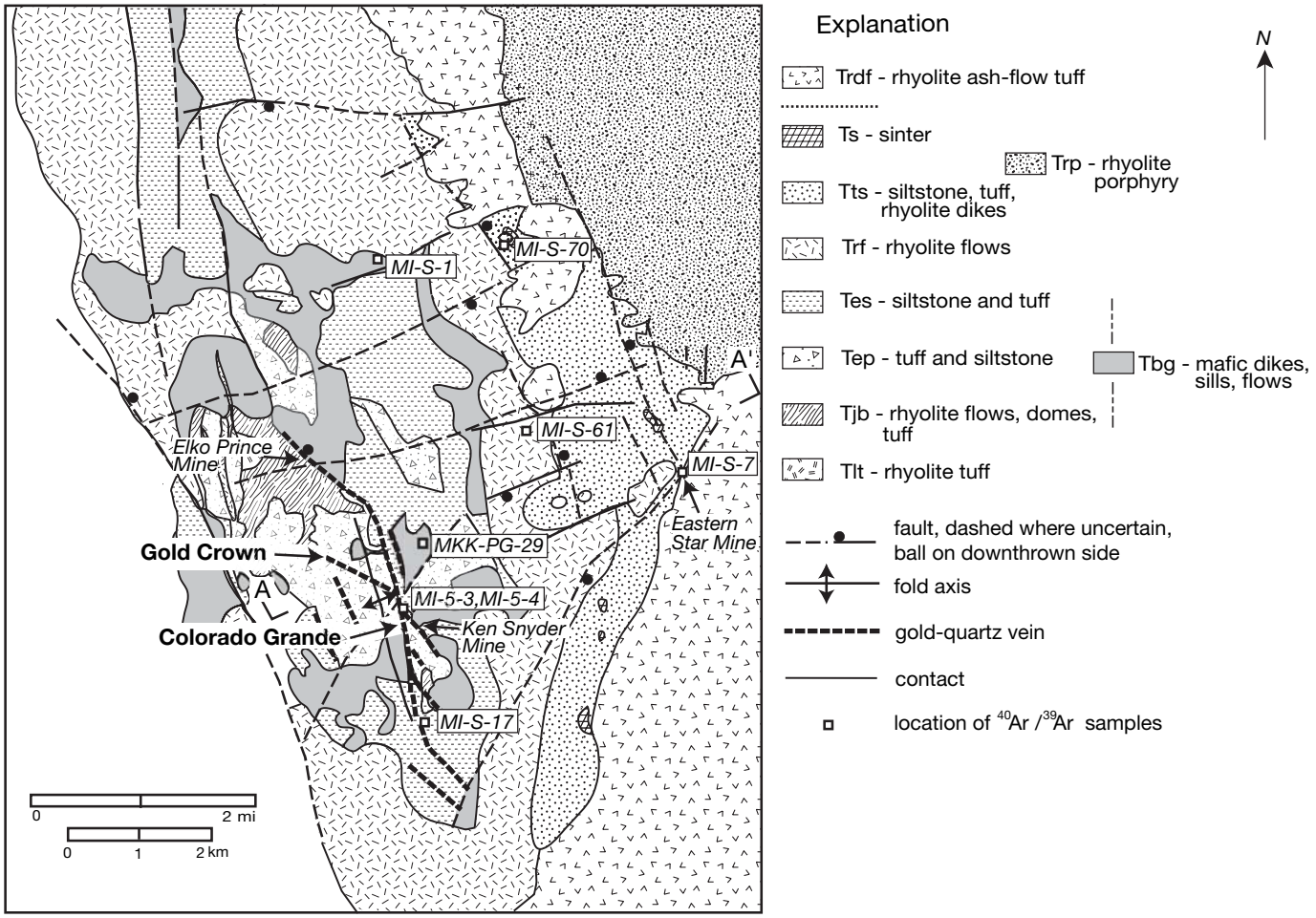

FIG. 3. Geology of the Midas area, southern Snowstorm Mountains. Geology modified from Wallace (1993), Goldstrand and Schmidt (2000), and unpublished mapping by P. Goldstrand, K. Schmidt, and S. Garwin (2002). Explanation of units shown in Figure 2. Locations of northeast-southwest cross section A-A' (Fig. 4) and samples used for $^{40}Ar/^{39}Ar$ dates shown.

members (Tes 1-5; Goldstrand and Schmidt, 2000; Fig. 2). Detrital fragments include minor sanidine and plagioclase that form ≤1 vol percent of the rock and clasts of Paleozoic quartzites. The tuff units contain plagioclase phenocrysts, 5 to 15 vol percent of the rock, in a fine-grained matrix. Amygdules contain chlorite, quartz, and calcite. Unlike the middle sedimentary member of the Elko Prince formation, the Esmeralda formation appears to be laterally continuous throughout the Midas area. The abundance of Paleozoic cobbles increases northeastward from the mine area and suggests a sediment source to the north-northeast where Paleozoic rocks are exposed (Goldstrand and Schmidt, 2000). In addition, Wallace (1993) has described clast imbrication that indicates a southwest transport direction.

Numerous mafic sills and dikes intrude, and flows are interbedded within, the felsic volcanic and volcaniclastic section described above. Basalt, basaltic andesite, diabase, and gabbro are dark gray-green to black (Tbg; Goldstrand and Schmidt, 2000). These rocks are mainly intrusive in the mine area; basaltic flows crop out north, west, and east of the mine (Wallace, 1993). Evidence for multiple episodes of mafic volcanism at Midas includes peperites in the intermediate member of the Elko Prince formation, dikes in overlying siltstones of the Esmeralda formation with sharp contacts indicating intrusion into relatively dry sediments with no resultant hydroclastites, and crosscutting intrusions and flows of the mafic units (Tbg). Peperites grade laterally into a feature described locally as a clastic dike. The dike is composed of siltstone to gritstone that is commonly vertically bedded near contacts with veins (Goldstrand and Schmidt, 2000). The dike is subparallel to a north-south–striking fault that contains the Colorado Grande vein. Emplacement of the clastic dike apparently was controlled by this fault and may be related to an episode of mafic magmatic activity coeval with deposition of sediments of the intermediate member of the Elko Prince formation. There are two distinct varieties of mafic volcanic rocks (Tbg), one with ilmenite as the main oxide and one with magnetite as the main oxide. Ilmenite-bearing mafic rocks locally intrude the magnetite-bearing mafic rocks which are more abundant at depth. Mafic flows or sills are also common within, and at the top of, sedimentary rocks of the overlying Esmeralda formation and represent a younger episode of

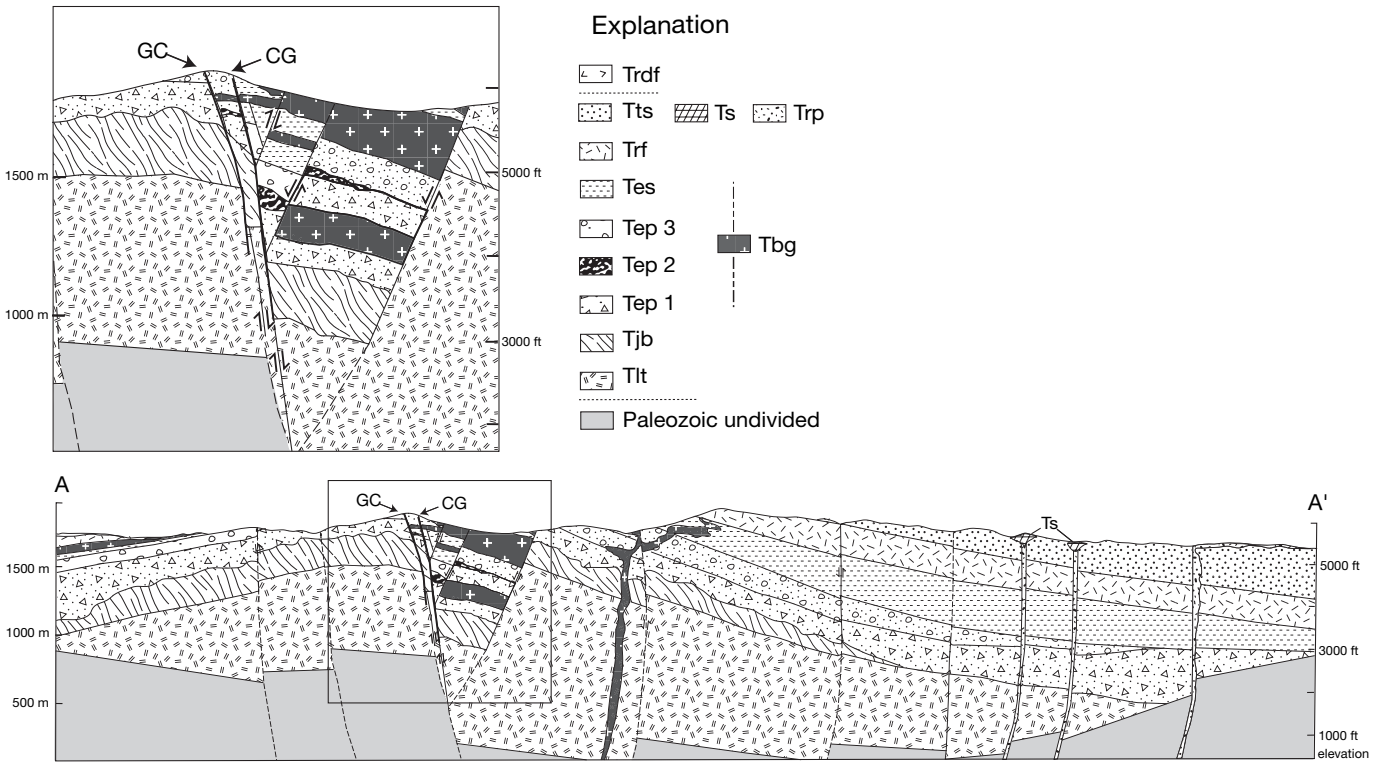

FIG. 4. Cross section A-A' of the Midas area. Explanation of units shown in Figures 2 and 3; location shown in Figure 3. CG = Colorado Grande vein, GC = Gold Crown vein. Vertical scale = horizontal scale.

mafic magmatic activity. Mafic dikes, sills, and flows are not present in the overlying tuffs and sedimentary rocks.

The red rhyolite (Trf) is composed of lava flows and ash-flow tuffs (Wallace, 1993). In the Midas area, these flows are red to grayish-white, banded, and sanidine bearing, and they are in depositional contact with the Esmeralda formation and basalts. A laterally widespread, east-dipping rhyolite flow caps a north-trending ridge approximately 1 km northeast of the mine and forms gently dipping slopes (Figs. 3–4). These rhyolites are weakly to strongly altered but are not known to host significant mineralization. The massive rhyolite contains phenocrysts of sanidine forming up to 5 vol percent of the rock and a trace of plagioclase in a devitrified matrix with axiolitic and spherulitic texture. North-northwest–striking, rhyolite feeder dikes are exposed in the northwestern portion of the Midas district (Wallace, 1993).

A unit composed of siltstones, tuffs, and rhyolite dikes conformably overlies and intrudes the red rhyolite. This unit (Tts) is exposed 2 km east of Midas and is up to 300 m thick (Figs. 3–4). At the base of the unit, thinly laminated siltstones, locally containing well-rounded clasts of Paleozoic quartzite, grade upward into tuffaceous and pumice-bearing siltstones and rhyolite tuffs. Rounded to angular clasts of chalcedony and opal and tuff breccias are interbedded within the upper portion of the sedimentary sequence. Several flow-banded, spherulitic rhyolite dikes intrude the sediments and grade laterally into hydrothermally altered breccias along their contacts. At the Eastern Star mine, 5 km east of the Ken Snyder mine (Fig. 3), banded gold-bearing quartz veins are hosted by a hydrothermally altered vent breccia with a rhyolite matrix, and a flow-banded spherulitic rhyolite dike crops out within 100 m of the mine workings. Approximately 5 km north-northeast of the main veins at Midas, sinter deposits (Ts) and hydrothermal vents are aligned along north-northwest–trending faults (unpub. mapping, P. Goldstrand, K. Schmidt, and S. Garwin, 2002; Fig. 3). The vents are marked by circular depressions, 10 to 30 m in diameter, ringed with brecciated opaline material. Adjacent to a series of these vents, laminated, gently dipping sediments were opalized close to the paleosurface of the fossil hydrothermal system that was active during formation of this unit. In the vicinity of the opalized rocks, conglomerates grade southward into lacustrine sedimentary rocks, indicating a south- to southeast-sloping paleotopography at the time of deposition (S. Garwin, pers. commun., 2002).

North and east of the Eastern Star mine, a sanidine- and quartz-rich rhyolite porphyry (Trp) occupies a fault or intrusive contact with the unit Tts (Figs. 3–4). Approximately 1 km north of Eastern Star, the porphyry is hydrothermally altered and hosts fractures containing opaline silica and cinnabar (Red Arrow claims; LaPointe et al., 1991). This porphyry is locally overlain by an ash-flow tuff described below.

Five km northeast of the Midas deposit, preserved on the flanks of a gentle fold, a relatively fresh, rhyolite ash-flow tuff (Trdf) with a thin, basal vitrophyre unconformably overlies opalized siltstones of Tts (Fig. 3). The tuff is part of a regionally recognized unit (rhyodacite of Fraser Creek; Wallace, 1993) that marks the end of significant hydrothermal activity

and mineralization at Midas. This unit locally cuts down into the underlying sedimentary sequence and lies directly on the red rhyolite; in places, the basal vitrophyre is absent. Overall, the unit thickens eastward (S. Garwin, pers. commun., 2002), indicating that the red rhyolite and overlying sedimentary sequence formed a topographic high to the west.

Within 5 km west of the Midas deposit several rhyolite and rhyodacitic ash-flow tuffs and associated flows were deposited above the red rhyolite (not shown in Fig. 3; Wallace, 1993). These units apparently did not extend eastward beneath the tuff of Trdf, possibly due to the intervening topographic high of red rhyolite in the vicinity of Midas (Wallace, 1993). Source vents for these units may have contributed ash to tuffaceous siltstones and tuffs (Tts) overlying the red rhyolite (Trf). The Sawtooth dike, which is located approximately 15 km southwest of Midas (Fig. 1b), was a feeder for some of these flows and tuffs (units Trpoi and Trpo of Wallace, 1993). Based on the stratigraphic position of the flows above the red rhyolite (Trf), the rhyolite dike and associated flows are interpreted to have been coeval with the rhyolite porphyry (Trp) east of Eastern Star. These rhyolites are similar texturally and contain abundant phenocrysts of sanidine and quartz.

Structural geology

The gold-bearing quartz veins and their host rocks formed during east-northeast– to west-southwest–oriented extension (Zoback and Thompson, 1978) and associated normal and oblique displacements along faults. The predominant fault orientations in the Midas district are N to N 30° W, N 50° W to N 60° W, and east to east-northeast (Blair, 1991; Wallace, 1993; Casteel et al., 1999; Goldstrand and Schmidt, 2000; Fig. 3). The Colorado Grande vein formed in a laterally and vertically persistent, north-south– to N30°W-striking, steeply northeast dipping normal fault. Subsidiary mineralized faults within the hanging wall display some reverse movement (Fig. 4). The Gold Crown vein formed in a steeply northeast dipping, N 50° to 60° W-striking fault that splays into the footwall of the Colorado Grande fault (Fig. 4). Fault splays of similar orientation in the hanging wall host additional veins (Casteel et al., 1999; Goldstrand and Schmidt, 2000).

The Colorado Grande fault was a long-lived growth fault. It controlled the distribution of lacustrine sediments of Tep 2 and intrusion of the clastic dike (Goldstrand and Schmidt, 2000). Offsets along the Colorado Grande fault indicate that normal displacement continued after deposition of the upper Esmeralda formation. Total normal displacement prior to mineralization may have been as much as 335 m (Goldstrand and Schmidt, 2000), with little normal movement after formation of the veins. A component of strike-slip along this fault resulted in the formation of a pull-apart basin (followed by deposition of unit Tep 2; Goldstrand and Schmidt, 2000), a reverse flower structure associated with the faults hosting the bonanza vein system and dilational openings along the main mineralized faults (D.A. Rhys, unpub. rept., 2002).

East- to northeast-striking faults that developed prior to and following mineralization are not known to host significant ore (Goldstrand and Schmidt, 2000). In the Midas region, additional postmineralization movement occurred along north-trending faults that deformed postmineralization volcanic rocks (e.g., unit Trdf; Wallace, 1993).

Host rocks of the veins dip gently away from a north-northwest–trending axis parallel to, and approximately 300 m west of, the Colorado Grande vein (Goldstrand and Schmidt, 2000; Fig. 4). Postmineralization rhyolites appear to terminate at the flanks of the shallow anticline (Wallace, 1993). Doming preceded development of the Midas hydrothermal system and may have been a product of emplacement of an intrusion at depth and/or faulting.

Hydrothermal alteration and vein formation

The alteration assemblages show a crude zonation centered on the main veins. Weak propylitic alteration occurs at distances greater than 400 m from the veins. Minor veining and partial replacement of phenocrysts and groundmass by chlorite, calcite, minor smectite (predominantly montmorillonite), and a trace of pyrite characterize this alteration. Regional weak propylitic alteration preceded main-stage alteration related to formation of the bonanza veins and near-surface hot spring activity.

Propylitic alteration intensifies toward the veins with an increased density of fracturing and veining and more complete replacement of phenocrysts and groundmass and/or matrix. Calcite, chlorite, pyrite, and smectite (montmorillonite and nontronite) are abundant. Albitization of plagioclase and adularization of sanidine are common. Moderate propylitic alteration grades into intense propylitic alteration within 50 to 100 m of the main veins and at depth. In zones of intense propylitic alteration, epidote and prehnite are variably present and are accompanied by increased abundances of calcite, pyrite, quartz, and adularia. Intense propylitic alteration grades into potassic alteration within 30 m of the main veins. In zones of potassic alteration, nearly complete replacement of phenocrysts and groundmass and/or matrix is accompanied by an increased density of veining. Abundances of adularia, pyrite, marcasite, smectite (montmorillonite and illite), quartz, chalcopyrite, and sphalerite increase, and abundances of chlorite decrease; chlorite is Fe rich. More intense potassic alteration commonly occurs within 20 m of the veins. In this zone, original textures are destroyed, and abundances of pyrite and/or marcasite increase. Illite ± sericite are slightly more abundant but overall present in trace amounts. Adjacent to the veins, wall rocks contain abundant silica and traces of selenide minerals. These phases were deposited during the earliest stages of the main ore-bearing veins.

Argillic alteration is most strongly developed in permeable volcaniclastic rhyolites (Tep and Tes), along faults, and at shallower levels of the deposit where it appears to overprint propylitic and potassic alteration. Phenocrysts and matrix are replaced by montmorillonite and minor kaolinite. Along the main faults, late deposition of montmorillonite, pyrite, calcite, and siderite in crosscutting veinlets followed formation of bonanza veins, possibly during collapse of the hydrothermal system.

The Colorado Grande and Gold Crown veins formed during multiple episodes of deposition and brecciation (Goldstrand and Schmidt, 2000; Leavitt, et al., 2000; D.A. Rhys, unpub. rept., 2002). Early silica flooding and brecciation of the wall rocks was followed by deposition of banded veins, several centimeters to several meters wide, which comprise high-grade ore. Dark bands variably enriched in electrum,

naumannite, chalcopyrite, pyrite, sphalerite, and minor galena, aguilarite, and marcasite alternate with quartz-, chalcedony-, adularia-, and calcite-rich bands. In any given vein, dark bands range in number from several to 20 (D.A. Rhys, unpub. rept., 2002). Bladed calcite, adularia and mosaic quartz are more abundant in earlier bands; pyrite and crystalline quartz are more abundant in later bands. During and following deposition of banded ore, several episodes of brecciation disrupted veins and wall rocks. Calcite and silica were deposited during and following these events.

Multiple episodes of silicification and vein formation are also evident at the Eastern Star mine. At Eastern Star, the mineralization is hosted by an intrusive or hydrothermal vent breccia that contains rounded fragments of Paleozoic cobbles, chalcedony, and angular volcanic rocks within a rhyolite matrix (Bentz et al., 1983; LaPointe et al., 1991). This breccia may have formed due to intrusion of rhyolite into a wet stream channel containing cobbles of chalcedony from earlier hydrothermal activity and Paleozoic cobbles from older (Tts) conglomerates. This breccia was later silicified and cut by steeply dipping, banded, quartz-adularia-calcite-selenide-electrum veins up to 10 cm wide.

$^{40}Ar/^{39}Ar$ Geochronology

Newly dated samples of volcanic rocks and mineralized veins at Midas provide constraints on the age of the host rocks and the age and duration of the mineralizing hydrothermal system. All dates described here were obtained by $^{40}Ar/^{39}Ar$ dating techniques. Although most rock samples were weakly altered, the effects of hydrothermal alteration were eliminated by handpicking and microscopic observation of mineral separates. Detailed sample descriptions and sample preparation and analytical techniques are described in Appendices 1 and 2.

Samples

Basalt and basaltic andesite (Tbg): Two samples of basalt and basaltic andesite (Tbg) were dated. One sample of basalt, MKK-PG-29, was collected 2 km northeast of the Ken Snyder mine (Fig. 3) where vesicular and glassy textures of some of the basalts, as well as field relationships, suggest that mafic lavas flowed onto a surface of Esmeralda formation sediments. A sample of basaltic andesite, MI-S-1, was collected several kilometers north-northwest of the Midas deposit from the same location as a sample dated previously using whole-rock, K-Ar methods (Wallace, 1993; Table 1). The basaltic andesite is overlain by siltstones of the Esmeralda formation and is either a flow or a sill. Separates of plagioclase phenocrysts were dated by step heating.

Upper Elko Prince formation (Tepu): Higher in the host rock sequence, a sample of the uppermost portion of the Elko Prince formation, MI-S-17, was obtained from an outcrop of airfall tuff (Tepu), 0.75 km south of the mine (Fig. 3). In outcrop Tepu overlies tuffs of the upper member of the Elko Prince formation (Tep 3). A separate of sanidine phenocrysts was dated by step heating.

Red rhyolite (Trf): A sample of the red rhyolite (Trf), MI-S-61, was collected from a north-trending ridge, 3 km northeast of the Ken Snyder mine (Fig. 3). At this location the rhyolite appears to be a flow. A separate of sanidine phenocrysts was dated by laser fusion.

Rhyolite tuff (Trdf): A sample of rhyolite tuff (Trdf), MI-S-70, was collected from an outcrop approximately 5 km northeast of the Ken Snyder mine (Fig. 3). At the base of the outcrop, the tuff contains shards of unaltered obsidian, sanidine, and sparse plagioclase. It grades upward into more crystal-rich zones. A lithophysal, reddish oxidized zone occurs at the top of the outcrop. Lithic fragments include rounded mafic lapilli and buff-colored chalcedony. A separate of sanidine phenocrysts from the crystal-rich portion of the tuff was dated by laser fusion.

Colorado Grande vein: Two samples of the Colorado Grande vein were collected to date high-grade Au-Ag mineralization at the Midas deposit. Samples were obtained from the same underground location (spiral 4, 5,250-ft level, 462 ft south), from outer and inner bands of the vein (MI-5-4 and MI-5-3, respectively); the banded portion of the vein was approximately 20 cm wide at this location. The outer bands are clearly older than the inner bands in outcrop, hand specimen, and thin section. Separates of adularia from these bands were dated by step heating.

Eastern Star vein: A sample of banded, gold-bearing quartz-adularia-selenide vein (MI-S-7) was collected from the Eastern Star mine (Fig. 3). The occurrence of adularia in this vein is similar to that in the samples of the Colorado Grande vein. A separate of adularia was dated by step heating.

Results

Most samples yielded ages with few artifacts of hydrothermal alteration, sample preparation, or other contaminants. The new dates are summarized in Table 1 along with previously published geochronologic data from the Midas district and vicinity. Data reduction, statistical analysis, and general interpretation techniques are presented in Appendix 2. Analytical data are tabulated in Appendix 3.

Basalt and basaltic andesite (Tbg): The plateaus for both samples give ages that are generally consistent with regional stratigraphic relationships. However, data from both samples yielded slightly discordant ages that may indicate the presence of excess argon (Table 1, Fig. 5a-d). For data such as these, the minimum ages defining the plateau are the best choice for an apparent age, and if excess argon is present in these steps, the age is a maximum.

Isochron analysis of data for sample MI-S-1 indicates the presence of a small amount of excess argon ($^{40}Ar/^{36}Ar = 338 \pm 22$ compared to the atmospheric value of 295.5). This sample also yielded a statistically valid isochron age of 8.2 ± 1.1 Ma (MSWD = 2.2; Fig. 5b). However, low radiogenic yield, corrections for Ca-derived isotopes, and large atmospheric argon correction errors in the $^{40}Ar/^{36}Ar$ ratio can produce isochrons with large errors. The resulting isochron age is inconsistent with both the district and regional geology. Step heating produced a plateau age of 15.9 ± 0.3 Ma from steps 5 through 10 (comprising 52% of gas released; Fig. 5a). The latter date, which represents a maximum age, has been assigned to this sample.

The statistically valid isochron age for sample MKK-PG-29 is 13.22 ± 0.15 Ma with an MSWD of 1.6 for plateau steps 1 through 5 (Fig. 5c-d, Table 1). The initial $^{40}Ar/^{36}Ar$ ratio of 306.0 ± 2.0 suggests the presence of minor excess argon. However, the geologic relationships are inconsistent with

TABLE 1. Isotopic Ages from the Midas District and Vicinity

Rock type/vein (unit)	Material dated	Location		Sample ID (this study)	K/Ar Age (Ma ± 1σ)	$^{40}Ar/^{39}Ar$ Age				
		Latitude	Longitude			Isochron	Total gas	(Ma ± 1σ) plateau	Mean	Weighted mean
Rhyolite tuff (Trdf)	Sanidine	41°17'21"N	116°45'27"W	MI-S-70		15.23 ± 0.10* (MSWD = 1.8)			15.48 ± 0.36	15.39 ± 0.08
Colorado Grande vein, Ken Snyder mine	*Adularia*	*41°14'35"N*	*116°46'39"W*					*15.26 ± 0.05*[1]		
Colorado Grande vein, Ken Snyder mine; outer band, sp4/5250S/462'	Adularia	41°14'38"N	116°46'41"W	MI-5-4[2]		15.30 ± 0.08* (MSWD = 1.3)	15.35 ± 0.08	15.30 ± 0.08		
Colorado Grande vein, Ken Snyder mine; inner band, sp4/5250S/462'	Adularia	41°14'38"N	116°46'41"W	MI-5-3[2]		15.37 ± 0.09* (MSWD = 1.8)	15.42 ± 0.08	15.38 ± 0.08		
Ivanhoe deep vein	*Adularia*	*41°07'0"N*	*116°33'48"W*					*15.38 ± 0.08*[3]		
Sawtooth dike (Trpoi)	*Anidine*	*41°11'36"N*	*116°55'42"W*		*14.3 ± 0.8*[4]			*15.39 ± 0.02*[5]		
Eastern Star vein	Adularia	41°15'38"N	116°43'23"W	MI-S-7		15.40 ± 0.09* (MSWD = 1.2)	15.33 ± 0.10	15.39 ± 0.10		
Mineralized vein in altered rhyolite	*Adularia*	*41°15'N*	*116°48'W*		*15.4± 0.8*[6]					
Rhyolite flow (Trf)	Sanidine	41°15'59"N	116°45'33"W	MI-S-61		15.63 ± 0.12* (MSWD = 0.31)			15.65 ± 0.05	15.65 ± 0.08
Fine-white tuff (Tepu)	Sanidine	41°14'05"N	116°46'23"W	MI-S-17		15.60 ± 0.09 (MSWD = 0.97)	15.91 ± 0.11	15.74 ± 0.11*		
Basaltic andesite (Tbg)	*Whole rock*	*41°16'55"N*	*116°47'32"W*		*14.7 ± 0.5*[7]					
Basaltic andesite (Tbg)	Plagioclase	41°16'55"N	116°47'32"W	MI-S-1		13.22 ± 0.15 (MSWD = 1.6; excess argon)	19.37 ± 0.26	15.9 ± 0.3 * (maximum age)		
Basalt (Tbg)	Plagioclase	41°14'35"N	116°45'25"W	MKK-PG-29[2]		8.2 ± 1.05 (MSWD = 2.2; excess argon)	17.59 ± 0.20	16.0 ± 0.2 * (maximum age)		

Notes: Nevada Isotope Geochronology Laboratory at the University of Nevada, Las Vegas data; preferred ages for samples from this study are marked with *; ages from other studies in italics; statistical methods used to determine dates for this study are as follows: Inverse isochron analysis routines (York, 1969) utilized to calculate isochron age; outliers omitted until MSWD <2.5; errors include J and MSWD; plateau ages required significant segment of gas released, or ≥50%, and contiguous steps or ages overlap at 2σ confidence level ; calculation of means and weighted means use model apparent ages and exclude analyses >2σ from the mean (Spell et al., 1996); sources of additional dates not determined in this study are described below; all ages reported using an age of 27.9 Ma for the Fish Canyon Tuff sanidine; original published ages shown in brackets below

[1] Goldstrand and Schmidt (2000) [15.23 ± 0.05 Ma; New Mexico Geochronology Research Laboratory]

[2] Data are from Leavitt et al. (2000)

[3] Peppard (2002) [15.34 ± 0.05 Ma; New Mexico Geochronology Research Laboratory]

[4] Wallace et al. (1990)

[5] Wallace (2003)

[6] McKee et al. (1976), recalculated to new decay constants (Steiger and Jager, 1977)

[7] Wallace and McKee (1994)

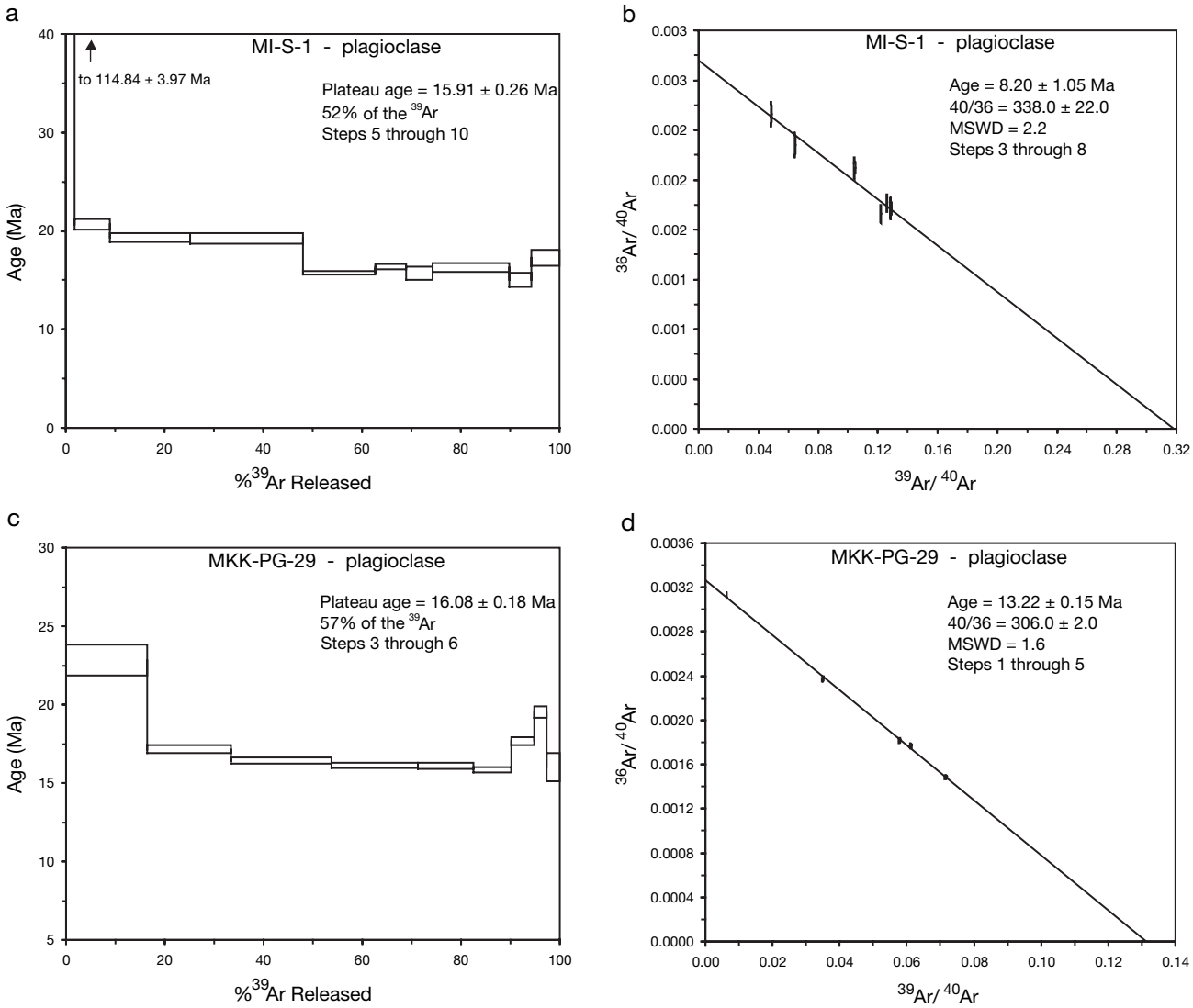

FIG. 5. Age spectra and isochron plots for $^{40}Ar/^{39}Ar$ step heating of plagioclase separates from basalts and basaltic andesites (Tbg). a. and b. Results of analyses of sample MI-S-1. c. and d. Results of analyses of sample MKK-PG-29. In the age spectra (a and c), the width of each apparent age is shown at $\pm 1\sigma$ uncertainty. Step-heating measurements began at 600°C, with subsequent measurements taken following increases of 100°C, to a maximum of 1,400°C (App. 3). Analyses defining the isochrons are marked with error shown at 2σ.

such a young age. Steps 3 to 6 of the age spectrum comprise ~57 percent of the total gas released and define a plateau which yields a weighted mean age of 16.0 ± 0.2 Ma. The latter age is consistent with the geologic relationships and has been assigned to this sample. The U-shaped age spectrum of MKK-PG-29 can be explained by the presence of excess argon throughout the sample (McDougall and Harrison, 1999). Because the high- and low-temperature steps have lower radiogenic yields, their ages are strongly affected by any excess argon.

Upper Elko Prince formation (Tepu): Step heating of sanidine from sample MI-S-17 yielded a total gas age of 15.91 ± 0.11 from 13 steps and a plateau age of 15.74 ± 0.11 from steps 4 through 13 (Table 1, Fig. 6a). The first several steps that contained abundant atmospheric argon may represent the effects of weak clay alteration of the outer rims of some sanidine crystals. An inverse isochron with all 13 steps yields an age of 15.60 ± 0.09, an initial $^{40}Ar/^{36}Ar$ of 305.9, and an MSWD of 0.97 (Fig. 6b); it demonstrates the large spread in radiogenic yield and appears to provide a reliable age. The isochron and plateau ages overlap within 1σ, and the isochron age has been assigned to this sample.

Red rhyolite (Trf): Laser fusion analysis of 10 sanidine grains from sample MI-S-61 yielded very homogeneous ages ranging from 15.62 to 15.72 Ma, a mean age of 15.65 ± 0.05 Ma, and a weighted mean age of 15.65 ± 0.08 Ma (Table 1, Fig. 6c). The highly radiogenic analyses cluster at one end of an inverse isochron, leaving the nonradiogenic argon poorly constrained (Fig. 6d). Nonetheless, the isochron yields an age of 15.63 ± 0.12 Ma, an initial $^{40}Ar/^{36}Ar$ of 315 ± 25, and an MSWD of 0.31. All 10 ages, which lie within $\pm 2\sigma$, are most likely representative of unaltered juvenile sanidines and

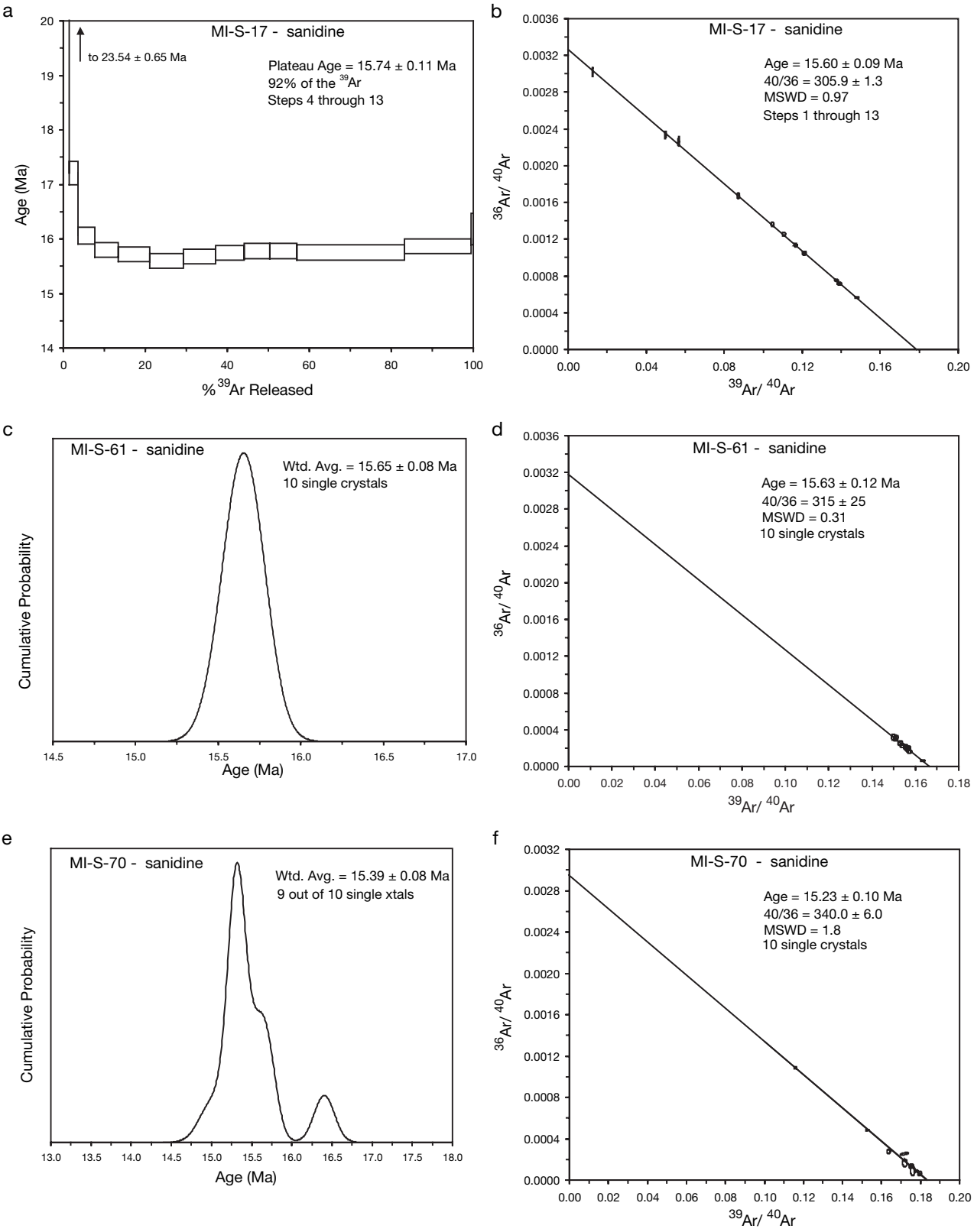

FIG. 6. Age spectra and cumulative probability and isochron plots for sanidine separates from pre- and postmineralization rhyolites. a. and b. Results of $^{40}Ar/^{39}Ar$ step heating of sanidine from the uppermost member of the Elko Prince formation (Tepu), sample MI-S-17. Analyses and plots were carried out as described for step-heated mineral separates in Figure 5. Laser-fusion $^{40}Ar/^{39}Ar$ analyses of 10 separate crystals were carried out for two samples. c. and d. Results of analyses of sample MI-S-61 from the red rhyolite (Trf). e. and f. Results of analyses of sample MI-S-70 from rhyolite tuffs (Trdf). Results are plotted on probability distribution diagrams (c and e) and isochron plots (d and f, as described in Fig. 5).

correspond to the age of eruption of the rhyolite flow or highly homogeneous tuff. The weighted mean and isochron ages are virtually identical within the limits of error, and the isochron age has been assigned to this sample.

Rhyolite tuff (Trdf): Fusion analysis of 10 sanidine crystals from sample MI-S-70 yielded a relatively heterogeneous population of apparent ages ranging from 15.00 to 16.40 Ma, with a mean age of 15.48 ± 0.36 Ma, and a weighted mean age of 15.39 ± 0.08 (Table 1, Fig. 6e). An inverse isochron with all 10 crystals yields an age of 15.23 ± 0.10, an initial $^{40}Ar/^{36}Ar$ of 340.0 ± 6.0, and an MSWD of 1.8 (Fig. 6f). The likelihood of excess argon and the presence of outliers in the population could indicate that either xenocrysts are present and/or that some of the sanidine crystals have been hydrothermally altered. For this sample, the isochron is considered the most reliable age.

Colorado Grande vein: Adularia separates from distinct mineralized bands of the Colorado Grande vein produced nearly ideal age spectra. The sample from an inner band, MI-5-3, gave a nearly ideal flat age spectrum with a plateau age of 15.38 ± 0.08 Ma from steps 2 through 8 (~75% of gas) and a total gas age of 15.42 ± 0.08 Ma (Table 1, Fig. 7a). Steps 1 through 6 define an isochron age of 15.37 ± 0.09 Ma, with no indication of excess argon and an acceptable MSWD of 1.8 (Fig. 7b). An isochron age, identical to the plateau age, has been assigned to this sample.

The adularia sample from an outer band, MI-5-4, also yielded a nearly ideal, flat age spectra with ~95 percent of the gas yielding identical ages with a plateau age of 15.30 ± 0.08 Ma from steps 2 through 10; the total gas age is 15.35 ± 0.08 (Fig. 7c). An isochron defined by steps 1 through 10 produced an age of 15.30 ± 0.08, with no indication of excess argon, and an MSWD of 1.3 (Fig. 7d).

Eastern Star vein: A sample of adularia from the banded vein, MI-S-7, yielded a nearly flat age spectrum with steps 4 through 11, defining a plateau age of 15.39 ± 0.10 Ma, and a total gas age from all steps of 15.33 ± 0.10 Ma (Table 1, Fig. 7e). Steps 1 through 8 define a statistically valid isochron age of 15.40 ± 0.09 Ma, with no excess argon and an MSWD of 1.2 (Fig. 7f). No excess argon is indicated, and thus the plateau and isochron ages are essentially identical. The isochron age has been assigned to this sample.

Summary of Geochronology of Midas Area

Newly determined ages of host rocks and gold-bearing quartz veins indicate that several units in the Midas area are older than previously thought and that high-grade mineralization was coeval with felsic volcanism. Results of geologic mapping, new dates from this study, and several additional isotopic dates for volcanic rocks and Au-Ag mineralization in the region are summarized in Table 1 and Figure 8. The new $^{40}Ar/^{39}Ar$ dates for the Midas area correlate well with stratigraphy in the Midas district.

The new $^{40}Ar/^{39}Ar$ ages of banded veins from throughout the Midas area are essentially identical. Adularia from the Colorado Grande vein, the Eastern Star mine, and Ivanhoe (Fig. 1b) yielded dates ranging from 15.3 ± 0.1 to 15.4 ± 0.1 Ma (Table 1). The 15.38 ± 0.08 Ma age of banded selenide-precious metal veins at Ivanhoe (Peppard, 2002), 20 km to the southeast of Midas, is the same as that of the Colorado Grande vein. The dates from the inner and outer bands of the Colorado Grande vein are indistinguishable at 1σ, suggesting that the vein formed over a relatively short period of time.

Field relationships indicate that basalts and basaltic andesites (Tbg) at Midas were emplaced multiple times during accumulation of the volcanic pile that hosted the hydrothermal system. The mafic volcanic rocks (Tbg) are similar in age or younger than the Esmeralda formation (Tes) and older than the red rhyolite (Trf). A maximum age of 15.9 ± 0.3 Ma for basalt sample MI-S-1 is consistent with an age of 15.6 ± 0.1 Ma for the overlying red rhyolite. A previous whole-rock, K-Ar analysis of a sample of this basalt from the same location as sample MI-S-1 yielded an age of 14.7 ± 0.5 Ma (Table 1; Wallace and McKee, 1994). This young age most likely reflects effects of minor alteration or glass in the groundmass and related loss of argon. The new $^{40}Ar/^{39}Ar$ dates indicate that mafic volcanism in the Midas district had waned prior to mineralization and are consistent with ages of mafic rocks elsewhere along the northern Nevada rift (e.g., ~16–15.8 Ma, Mule Canyon sequence; John et al., 2003).

The date of the fine-grained white tuff (Tepu) provides an upper limit of 15.6 Ma on the age of the Elko Prince formation (Tep). The Elko Prince formation was deposited at the same time that lacustrine and alluvial sedimentation took place 15 km to the southeast in the Ivanhoe area (Wallace, 2003). The aerially restricted distribution of the middle member (Tep 2), as well as more abundant ash-flow and lapilli tuffs at Midas compared to the Ivanhoe area, suggests localized basin formation at Midas during this time and closer proximity to a source.

The ages of the fine-grained white tuff (Tepu) and the red rhyolite (Trf) constrain deposition of the Esmeralda volcaniclastic sequence (Tes) to a period of less than 200 kyr (Table 1). The Esmeralda formation correlates with the middle phase of middle Miocene lacustrine sedimentation in the northern part of the Ivanhoe district (Wallace, 2003).

The date of 15.6 ± 0.1 Ma of the red rhyolite (Trf) confirms that this unit was erupted prior to mineralization and agrees with a new $^{40}Ar/^{39}Ar$ age of 15.4 Ma for the Sawtooth dike (Table 1; Wallace, 2003); the red rhyolite (Trf) is stratigraphically lower than rhyolite flows fed by the Sawtooth dike. The new age of the Sawtooth dike revises an age of 14.3 ± 0.8 Ma that was based on a K-Ar date of sanidine phenocrysts from the dike (Wallace et al., 1990) and shows that this intrusion and related flows, which extend to within 3 km west of Midas, are the same age as mineralization at Midas (Table 1; Wallace, 2003).

The tuffs, tuffaceous siltstones, and hydrothermal breccias of the unit Tts, lying between the red rhyolite (Trf) and unaltered tuffs (Trdf), accumulated between 15.6 ± 0.1 and 15.2 ± 0.1 Ma (dates of Trf and Trdf, respectively) and represent the youngest rocks affected by the hydrothermal system. Following deposition, these rocks and underlying units were tilted, and normal faulting took place along the main ore-bearing structures. Oblique-slip faulting and high-grade mineralization then took place at 15.4 Ma. The Tts unit is correlative with a middle sequence of sedimentary and volcaniclastic rocks described in the Ivanhoe area that was deposited between 15.6 and 15.2 Ma (Wallace, 2003). At this time, the Midas and Ivanhoe areas experienced felsic volcanism,

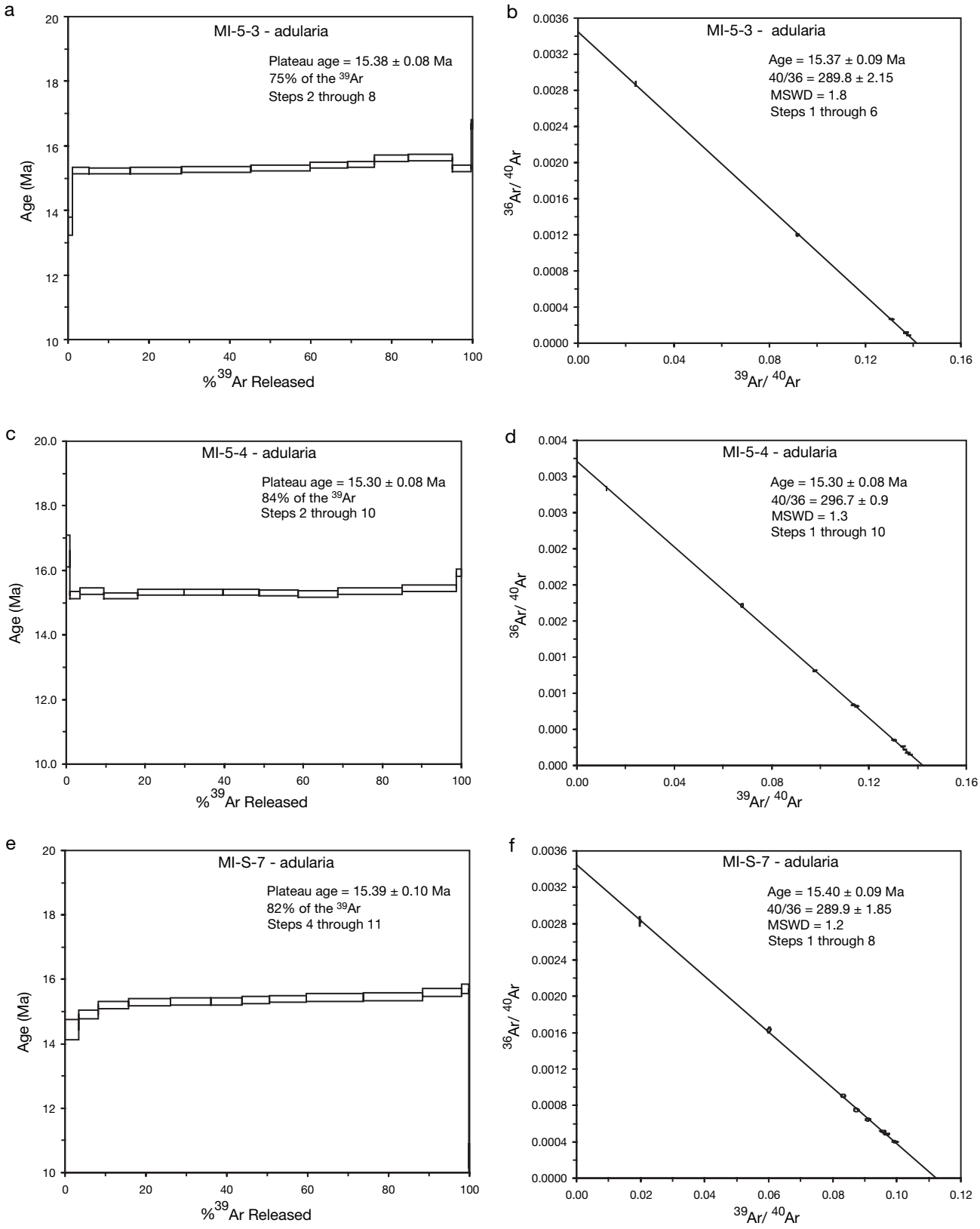

FIG. 7. Age spectra and isochron plots for $^{40}Ar/^{39}Ar$ step heating of adularia separates from high-grade Au-Ag veins. a. and b. Results of analyses of sample MI-5-3, an inner band of the Colorado Grande vein, Ken Snyder mine. c. and d. Results of sample MI-5-4, an outer band from the same location. e. and f. Results of analysis of sample MI-S-7 from a banded precious metal vein at the Eastern Star prospect. Analyses and plots were carried out as described in Figure 5.

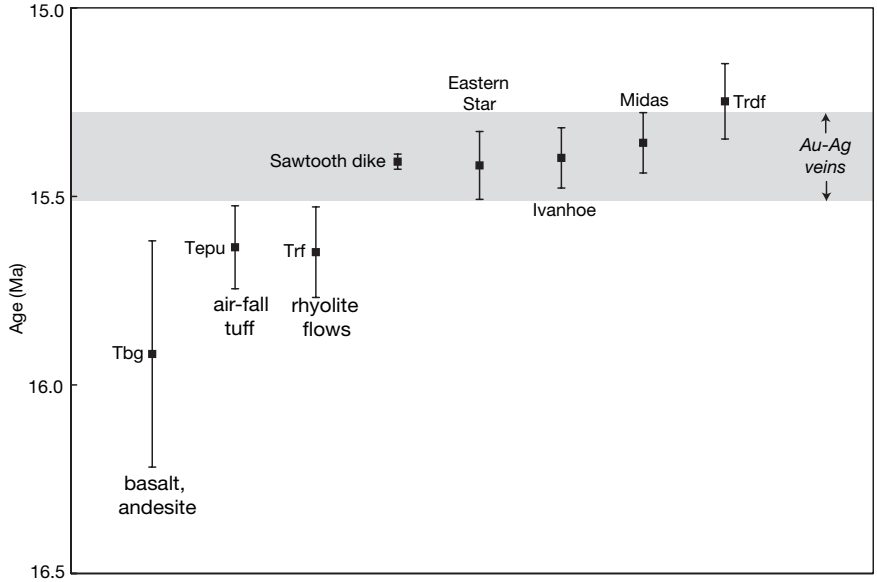

FIG. 8. Summary of geochronology of volcanic rocks and banded quartz-adularia-Au-Ag veins in the Midas area. Ages are plotted with squares, and errors are plotted as $\pm 1\sigma$ bars extending from squares. Rock units identified in Figure 2. The plot suggests that mafic volcanism waned by approximately 15.6 Ma and was followed by felsic-dominated volcanism. Rhyolite porphyries were coeval with high-grade precious metal mineralization at 15.4 Ma.

faulting, lacustrine sedimentation, hot spring activity, and Au-Ag-Hg mineralization.

Deposition of an ash-flow tuff (Trdf), which followed tilting and mineralization, is similar in age to rhyolite volcanism that occurred in the Ivanhoe area between 15.4 and 15.2 Ma (Wallace, 2003). At Midas, the lack of hydrothermal alteration in this unit shows that hydrothermal activity had ceased by about 15.2 Ma, similar to Ivanhoe (Wallace, 2003).

Duration of Hydrothermal System and Temporal Relationship between Volcanism and Mineralization

Although the absolute age of the onset of the Midas hydrothermal system is not known, the age of the red rhyolite (Trf) establishes a possible maximum age of 15.6 ± 0.1 Ma (sample MI-S-61; Table 1). The age of the capping, unaltered tuff (Trdf) provides a minimum age of the hydrothermal system of 15.2 ± 0.1 Ma (sample MI-S-70; Table 1). Thus, a tentative maximum duration of the hydrothermal system is 600 kyr. The ages of high-grade veins from the Midas region range from 15.4 ± 0.1 Ma (Eastern Star, sample MI-S-7; Colorado Grande, sample MI-5-3; and Ivanhoe; Table 1) to 15.3 ± 0.1 Ma (Colorado Grande, sample MI-5-4; Table 1) and show that banded, selenide-, Au-Ag–rich veins were deposited during a short-lived regional event that probably lasted less than 300 kyr.

High-grade Au-Ag veins at the Ken Snyder mine are 100 to 400 kyr younger than the youngest dated host rocks (Trf; samples MI-5-3, MI-5-4, and MI-S-61; Table 1). The age of gold-bearing quartz veins at the Eastern Star mine shows that as little as 20 kyr may have elapsed between the eruption of host rocks and deposition of precious metals (samples MI-S-7 and MI-S-61; Table 1). High-grade mineralization at Midas was roughly coeval with nearby rhyolite activity (15 km to the Sawtooth dike and 20 km to the Craig rhyolite in the Ivanhoe area; Wallace, 2003). The plutonic source of these rhyolites may have been the heat source for the hydrothermal system at Midas.

Comparison to Other Low-Sulfidation Hydrothermal Systems

At Midas, no more than 400 kyr elapsed between host-rock volcanism and the onset of mineralization. At Round Mountain hydrothermal activity and mineralization began within 500 kyr of ash-flow tuff eruption (Henry et al., 1997). At the Sleeper deposit, high-grade Au-Ag, banded quartz-adularia veins formed 100 to 300 kyr after eruption of the host rhyolite porphyry (Conrad and McKee, 1996). And, at the Mule Canyon deposit, hydrothermal alteration and Au-Ag deposition took place approximately 200 kyr after formation of the mafic volcanic host rocks (John et al., 2003).

Unaltered rhyolite tuffs and flows deposited shortly after the cessation of hydrothermal activity provide limits on the duration of low-sulfidation hydrothermal systems including Round Mountain, Sleeper, Ivanhoe, and Midas. At Round Mountain (Henry et al., 1997) and Midas, tuffs were deposited on or close to the paleosurface of the hydrothermal system. Similarly, the Sleeper deposit formed shortly before or during eruption of peralkaline tuffs of the McDermitt volcanic field, 20 to 50 km to the north, and may have been covered by tuffs during or following mineralization, although the tuffs do not presently overlie mineralized rocks (Conrad and McKee, 1996). At Ivanhoe, a rhyolite porphyry and flows capped a silicified, Hg-bearing tuff (Wallace, 2003).

These observations and new $^{40}Ar/^{39}Ar$ data in this study show that these hydrothermal systems were active for <100 to 700 kyr. The Midas hydrothermal system may have been active for up to 600 kyr and the main mineralizing event for up to 300 kyr. The Round Mountain hydrothermal system was

active for as little as 50 and no more than 500 kyr (Henry et al., 1997). The Mule Canyon hydrothermal system was active for up to 450 kyr (John et al., 2003). The Ivanhoe hydrothermal system was active for up to 350 kyr (Wallace, 2003). At Sleeper the main stage of mineralization and formation of banded Au-Ag veins took place over a period of up to 700 kyr (Conrad and McKee, 1996).

Active geothermal systems in the Taupo Volcanic Zone in New Zealand provide analogues of low-sulfidation epithermal systems (Hedenquist and Lowenstern, 1994; Simmons, 1995; Cooke and Simmons, 2000). Modeling of the Waiotapu system in New Zealand indicates that approximately 1 to 6 Moz of Au could be deposited in 10 kyr (Henley and Hedenquist, 1986). More recent measurements of deep fluid compositions along the Taupo Volcanic Zone support this model (Simmons and Brown, 2002). Current estimates of reserves and resources combined with past production suggest that the Midas-Ivanhoe region contained a minimum of approximately 4 Moz of Au and 40 Moz of Ag in high-grade quartz veins and probably an equal amount in altered and mineralized areas but outside the main vein zones. The high-grade veins formed during a pulse of mineralization that spanned up to 300 kyr. By analogy with New Zealand geothermal systems, the Midas hydrothermal system easily could have produced the estimated quantities of precious metals within this amount of time.

Model of Magmatic and Hydrothermal Evolution of Midas Area

Characterization of the timing of hydrothermal mineralization and volcano-tectonic events at Midas provides insights into the nature of formation of world-class epithermal ore deposits. A series of schematic cross sections (Fig. 9) illustrate the volcano-tectonic evolution of the Midas district. A thick section of felsic tuff, flow-dome complexes, and volcaniclastic and lacustrine sediments and mafic rocks accumulated in a deep graben and was periodically faulted and intruded by basalts and basaltic andesites (Fig. 9a-c). Following deposition of rhyolite flows, the volcanic rocks were gently folded, intruded by rhyolites, and faulted (Fig. 9d). Subsequent deposition of tuffaceous and opalized sediments and sinter deposits coincided with intrusion of rhyolite, development of the hydrothermal system, and formation of gold-bearing quartz veins along the main faults (Fig. 9d). After cessation of hydrothermal activity, continued tilting, erosion, and deposition of a postmineral tuff took place (Fig. 9e). Geologic events that led to development of high-grade veins in the Midas region include the following:

1. The Midas hydrothermal system developed after mafic volcanism waned and during rift-related felsic-dominated volcanism. The revised geochronology of the Midas area shows that several units of rhyolite previously thought to postdate mineralization and represent a younger bimodal sequence instead are coeval with mineralization (Fig. 9d). Overlying unaltered tuff (Fig. 9e) is older than previously recognized and only slightly younger than mineralization. A similar temporal association between gold mineralization and rhyolite volcanism has been observed in the Midas region at Ivanhoe (Wallace, 2003). The documentation of a close temporal and

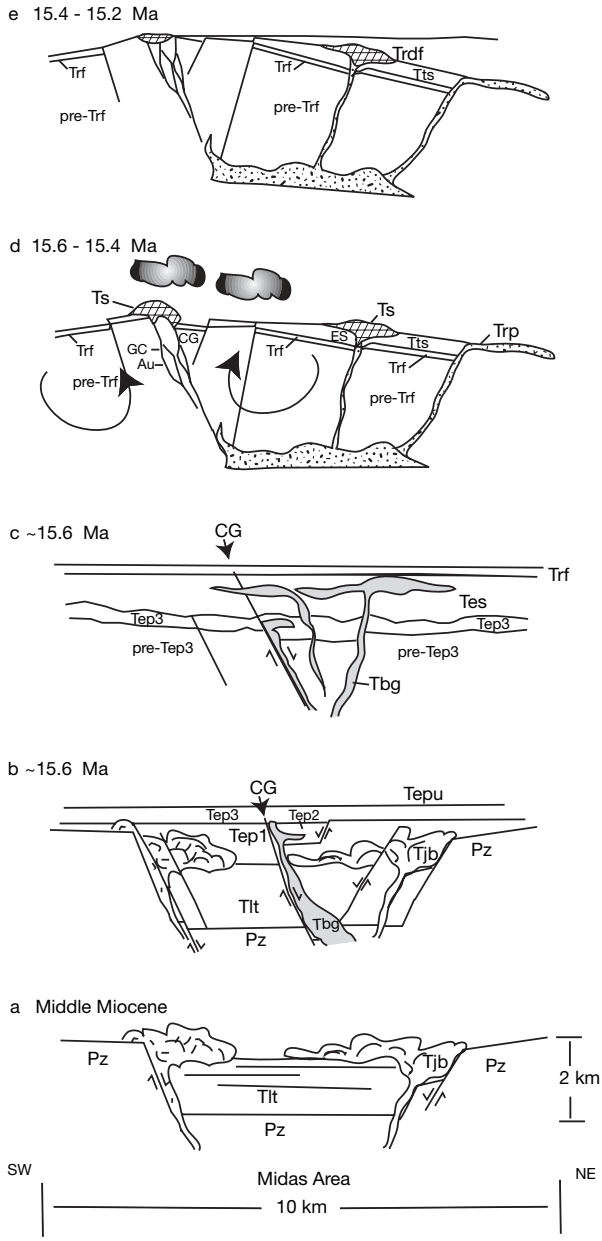

FIG. 9. Schematic northeast-southwest cross sections showing volcano-tectonic evolution of Midas district. a. Accumulation of ash-flow tuffs and underlying tuffaceous sediments of the lower tuff (Tlt) and the June Belle rhyolite flow-dome complexes (Tjb) within a deep graben in the Midas area during the middle Miocene. b. Continued faulting, deposition of lithic and lapilli tuffs and lacustrine sediments of the Elko Prince formation (Tep), and intermittent intrusion of basalts and basaltic andesites (Tbg). Movement along the ancestral Colorado Grande (CG) structure. Section capped by airfall tuff (Tepu). c. Continued intrusion and extrusion of basalts and basaltic andesites, accumulation of silicic airfall tuffs, and broadening of sedimentary basins during deposition of the Esmeralda formation (Tes). Continued movement along the CG structure. Deposition of rhyolite flows (Trf) on top of lacustrine sediments and mafic sills and flows. d. Gentle tilting, erosion, and accumulation of tuffaceous sediments along flanks of gentle fold. Intrusion of rhyolite porphyries in the Midas area. Development of hydrothermal system and fluid flow focused along major faults. Phreatic and magmatic eruptions along north-northwest–trending faults near Eastern Star (ES) and accumulation of sinter (Ts) and opalized sediments (Tts). Oblique-slip movement along main faults and emplacement of bonanza veins. e. Continuation of tilting, erosion, cessation of hydrothermal system, and deposition of postmineral ash-flow tuffs (Trdf).

spatial association of mineralization with felsic volcanism suggests that felsic intrusions provided a heat source to drive convection of hydrothermal fluids and possibly provided metals or other components.

2. Gentle tilting and faulting during the felsic-dominated volcanism provided plumbing for fluid flow. Gently dipping flows of the relatively impermeable red rhyolite (Trf) near the paleosurface probably formed a cap to the hydrothermal system that was breached locally by normal faults. Normal faults facilitated fluid upflow (Fig. 9d).

3. Shallow lakes were present in the vicinity of Midas sporadically during formation of the host rocks. During hydrothermal activity, water from the lakes probably recharged the meteoric water-dominated system (cf. Wallace, 2003). As hypothesized for other similar-aged epithermal precious metal deposits in Nevada, a period of increased rainfall may have enhanced the hydrothermal system (Berger and Henley, 1989; Wallace, 2003).

4. The nearly synchronous deposition of high-grade selenium- and Au-Ag–rich veins throughout the Midas area, including the Midas veins, Eastern Star, and Ivanhoe, at 15.4 Ma suggests that the metals were derived from the same hydrothermal system and that common depositional mechanisms operated. At Midas, the thickest portions of these high-grade veins occur in dilational zones created by oblique-slip motion along a north-northwest– to northwest-striking fault system (Fig. 9d). Evidence of coeval faulting and high-grade mineralization suggests that seismic events may have triggered movement along preexisting zones of weakness along the margins of the rift with release of fluids from deeper hydrothermal reservoirs. The presence of bladed calcite and adularia in gold-bearing quartz veins are indicative of boiling, possibly caused by the decreased pressure along faulted pathways (e.g., Sibson, 1987; Henley and Adams, 1992).

Conclusions

The high-grade Au-Ag veins at Midas were deposited no more than 400 kyr after eruption of the youngest volcanic host rocks and are only slightly older than overlying fresh tuffs. In the Midas region high-grade Au-Ag veins formed within a period of 300 kyr, athough hydrothermal activity may have lasted much longer. By analogy with active low-sulfidation geothermal systems, the estimated precious metal content of veins easily could have been deposited within this time frame. New dates of volcanic rocks show that sinters and opalized sediments formed on the paleosurface of the Midas hydrothermal system and that Au-Ag mineralization was coeval with felsic volcanism.

High-grade Au-Ag veins were deposited after a change from mafic-dominated bimodal volcanism and basin development to felsic volcanism, faulting, and local uplift. The similar ages of in situ rhyolite and mineralization suggest that they are genetically linked and that felsic volcanism and tectonic events led to the formation of high-grade selenium- and Au-Ag–rich bonanza veins in the Midas district.

Acknowledgments

Initial funding for this study was provided by a grant from Franco-Nevada Mining Corporation, facilitated by Ken Snyder. Additional funding was provided by the University of Nevada, Reno; Newmont Mining Corporation; student grants from the Society of Economic Geologists and the Geological Society of America; and the Woman's Auxiliary to the American Institute of Mining, Metallurgical and Petroleum Engineers, Inc. Steve Garwin, Jack Bernard, and Kirk Schmidt shared ideas and unpublished geologic mapping of the Midas district. Mike Ressel helped early on with preparation of mineral separates. Chris Henry provided expertise in petrography and geochronology. Reviews of earlier versions of this manuscript by Alan Wallace, Steve Garwin, Shane Ebert, Paul Layer, Byron Berger, David John, and Mark Hannington greatly improved the final paper. Jim, Will, Julia, and Jenny Leavitt gave additional support and encouragement.

May 14, 2003; September 16, 2004

REFERENCES

Albino, G.V., and Margolis, J., 1991, Differing styles of adularia-sericite epithermal deposits—contrasts in geologic setting and mineralogy [abs.]: Geological Society of America Abstracts with Program, v. 23, no. 5, p. A230.

Bentz, J.L., Tingley, J.V., Smith, P.L., and Garside, L.J., 1983, A mineral inventory of the Elko resoure area: Nevada Bureau of Mines and Geology Open-File Report 83-9, p. 1–6.

Berger, B.R., and Henley, R.W., 1989, Advances in the understanding of epithermal gold-silver deposits, with special reference to the western United States: Economic Geology Monograph 6, p. 405–423.

Blair, K.R., 1991, Geology of the Gold Circle district, Elko County, Neavda: Unpublished M.Sc. thesis, Tucson, University of Arizona, 85 p.

Blakely, R.G., and Jachens, R.C., 1991, Regional study of mineral resources in Nevada— insights from three-dimensional analysis of gravity and magnetic anomalies: Geological Society of America Bulletin, v. 103, p. 795–803.

Bonham, H.F., Jr., 1988, Models for volcanic-hosted epithermal precious metal deposits, *in* Schafer, R.W., Cooper, J.J., and Vikre, P.G., eds., Bulk mineable precious metal deposits of the western United States. Symposium proceedings: Reno, Geological Society of Nevada, p. 259–271.

Casteel, M.V., Schmidt, K, Goldstrand, P., Bernard, J., and Sandberg, J., 1999, Geologic setting of the Ken Snyder gold and silver mine, Elko, County, Nevada: Geological Society of Nevada Special Publication 29, p. 213–220.

Cebula, G.T., Kunk, M.J., Mehnert, H.H., Naeser, C.W., Obradovich, J.D., and Sutter, J.G., 1986, The Fish Canyon Tuff, a potential standard for the $^{40}Ar/^{39}Ar$ and fission-track dating methods [abs.]: Terra Cognita, Abstracts, v. 6, p. 139.

Christiansen, R.L., and Yeats, R.S., 1992, Post-Laramide geology of the U.S. Cordilleran region: Geological Society of America, Geology of North America, v. G-3, p. 261–406.

Connors, K.A., Noble, D.C., Bussey, S.D., and Weiss, S.I., 1993, Initial gold contents of silicic volcanic rocks: Bearing on the behavior of gold in magmatic systems: Geology, v. 21, p. 937–940.

Conrad, J.E., and McKee, E.H., 1996, High-precision $^{40}Ar/^{39}Ar$ ages of rhyolite host rock and mineralized veins at the Sleeper deposit, Humboldt County, Nevada: Geology and Ore deposits of the American Cordillera, Geological Society of Nevada Symposium, Reno/Sparks, Nevada, April 1995, Proceedings, p. 257–262.

Cooke, D.R., and Simmons, S.F., 2000, Characteristics and genesis of epithermal gold deposits: Reviews in Economic Geology, v. 13, p. 221–244.

Deino, A.L., and Potts, R., 1990, Single-crystal $^{40}Ar/^{39}Ar$ dating of the Olorgesailie Formation, southern Kenya rift: Journal of Geophysical Research, v. 95, p. 8453–8470.

Dickinson, W.R., 2002, The Basin and Range province as a composite extensional domain: International Geology Review, v. 44, p. 1–38.

Emmons, W.H., 1910, A reconnaissance of some mining camps in Elko, Lander, and Eureka Counties, Nevada: U.S. Geological Survey Bulletin 408, p. 47–57.

Glen, J.M.G., and Ponce, D.A., 2002, Large-scale fractures related to inception of the Yellowstone hotspot: Geology, v. 30, p. 647–650.

Goldstrand, P.M., and Schmidt, K.W., 2000, Geology, mineralization, and ore controls at the Ken Snyder gold-silver mine, Elko county, Nevada: Geological Society of Nevada, Geology and Ore Deposits 2000: the Great Basin

and Beyond Symposium, May 15–18, 2000, Reno-Sparks, Nevada, Proceedings, p. 265–287.
Heald, P., Foley, N.K., and Hayba, D.O., 1987, Comparative anatomy of volcanic-hosted epithermal deposits: Acid sulfate and adularia-sericite types: ECONOMIC GEOLOGY, v. 82, p. 1–26.
Hedenquist, J.W., and Lowenstern, J.B., 1994, The role of magmas in the formation of hydrothermal ore deposits: Nature, v. 370, p. 519–527.
Hedenquist, J.W., Arribas, A.R., and Gonzalez-Urien, E., 2000, Exploration for epithermal gold deposits: Reviews in Economic Geology, v. 13, p. 245–277.
Henley, R.W., and Adams, D.P.M., 1992, Strike-slip fault reactivation as a control on epithermal vein-style gold mineralization: Geology, v. 20, p. 443–446.
Henley, R.W., and Hedenquist, J.W., 1986, Introduction to the geochemistry of active and fossil geothermal systems: Monograph Series on Mineral Deposits 26, p. 1–22.
Henry, C.D., and Wolff, J.A., 1992, Distinguishing strongly rheomorphic tuffs from extensive silicic lavas: Bulletin of Volcanology, v. 54, p. 171–286.
Henry, C.D., Elson, H.B., McIntosh, W.C., Heizler, M.T., and Castor, S.B., 1997, Brief duration of hydrothermal activity at Round Mountain, Nevada, determined from $^{40}Ar/^{39}Ar$ geochronology: ECONOMIC GEOLOGY, v. 92, p. 807–826.
Izawa, E., Urashima, Y., Ibaraki, K., Suzuki, R., Yokoyama, T., Kawasaki, K., Koga, A., and Taguchi, S., 1990, The Hishikari gold deposit: High-grade epithermal veins in Quaternary volcanics of southern Kyushu, Japan: Journal of Geochemical Exploration, v. 36, p. 1–56.
John, D.A., 2001, Miocene and early Pliocene epithermal gold-silver deposits in the northern Great Basin, western United States: Characteristics, distribution, and relationship to magmatism: ECONOMIC GEOLOGY, v. 96, p. 1827–1853.
John, D.A., and Wallace, A.R., 2000, Epithermal gold-silver mineral deposits related to the northern Nevada rift: Geological Society of Nevada, Geology and Ore Deposits 2000: the Great Basin and Beyond Symposium, May 15–18, 2000, Reno-Sparks, Nevada, Proceedings, p. 155–175.
John, D.A., Garside, L.J., and Wallace, A.R., 1999, Magmatic and tectonic setting of late Cenozoic epithermal gold-silver deposits in northern Nevada, with an emphasis on the Pah Rah and Virginia Ranges and the northern Nevada rift: Geological Society of Nevada Special Publication 29, p. 64–158.
John, D.A., Wallace, A.R., Ponce, D.A., Fleck, R.J., and Conrad, J.E., 2000, New perspectives on the geology and origin of the northern Nevada rift: Geological Society of Nevada, Geology and Ore Deposits 2000: the Great Basin and Beyond Symposium, May 15–18, 2000, Reno-Sparks, Nevada, Proceedings, p. 127–154.
John, D.A., Hofstra, A.H., Fleck, R.J., Brummer, J.E., and Saderholm, E.C., 2003, Geologic setting and genesis of the Mule Canyon low-sulfidation epithermal gold-silver deposit, north-central Nevada: ECONOMIC GEOLOGY, v. 98, p.425–463.
LaPointe, D.D., Tingley, J.V., and Jones, R.B., 1991, Mineral resources of Elko County, Nevada: Nevada Bureau of Mines and Geology Bulletin 106, p. 162–168..
Leavitt, E.D., 2001, Hydrothermal alteration and geochronology of the Colorado Grande vein, Ken Snyder mine, Elko County, Nevada: Ralph J. Roberts Center for Research in Economic Geology Annual Research Meeting 2000, Feb. 7–8, 2001, Program and Reports, 15 p.
Leavitt, E.D., Goldstrand, P., Schmidt, K., Wallace, A.R., Spell, T., and Arehart, G.B., 2000, Geochronology of the Midas gold-silver deposit and its relationship to volcanism and mineralization along the northern Nevada rift: Geological Society of Nevada Symposium, Reno, 2000, Field Trip Guidebook 8, p. 157–162.
Leavitt, E., Spell, T.L., Wallace, A.R., Goldstrand, P., and Arehart, G.B., 2003, Volcano-tectonic setting of the Midas epithermal vein deposit, Elko County, Nevada [abs.]: Geological Society of America Abstracts with Programs, v. 35, no. 4, p. 61.
Ludington, S., Cox, D.P., Moring, B.C., and Leonard, K.W., 1996, Cenozoic volcanic geology of Nevada: Nevada Bureau of Mines and Geology Open-File Report 96-2, p. 5-1 to 5-10.
Ludwig, K.R., 1992, ISOPOLOT—a plotting and regression program for radiogenic-isotope data version 2.57: U.S. Geological Survey Open-file Report 91-445, 40 p.
McDougall, I., and Harrison, T.M., 1999, Geochronology and thermochronology by the $^{40}Ar/^{39}Ar$ method, 2nd ed.: New York, Oxford University Press, 269 p.
McKee, E.H., Tarshis, A.L., and Marvin, R.F., 1976, Summary of radiometric ages of Tertiary volcanic and selected plutonic rocks in Nevada. Part V, Northeastern Nevada: Isochron/West, no. 16, p. 15–27.
Naito, K., 1993, Occurrences of quartz veins in the Hishikari gold deposits, southern Kyushu, Japan: Resource Geology Special Issue 14, p. 37–45.
Noble, D.C., McCormack, J.K., McKee, E.H., Silberman, M.L., and Wallace, A.B., 1988, Time of mineralization in the evolution of the McDermitt caldera complex, Nevada-Oregon, and the relation of middle Miocene mineralization in the northern Great Basin to coeval regional basaltic magmatic activity: ECONOMIC GEOLOGY, v. 83, p. 859–863.
O'Neil, J.R., and Silberman, M.L., 1974, Stable isotope relations in epithermal Au-Ag deposits: ECONOMIC GEOLOGY, v. 69, p. 902–909.
Peppard, B., 2002, Geology and geochemistry of the Ivanhoe vein system, Elko, Nevada: Unpublished M.Sc. thesis, Ann Arbor, University of Michigan, 49 p.
Ponce, D.A., and Glen, J.M.G., 2002, Relationship of epithermal gold deposits to large-scale fractures in northern Nevada: ECONOMIC GEOLOGY, v. 97, p. 3–9.
Rott, E.H., 1931, Ore deposits of the Gold Circle district, Elko County: Nevada University Bulletin, v. 25, no. 5 (Nevada Bureau of Mines and Geology Bulletin 12), 30 p.
Sibson, R.H., 1987, Earthquake rupturing as a mineralizing agent in hydrothermal systems: Geology, v. 15, p. 701–704.
Sillitoe, R.H., and Hedenquist, J.W., 2003, Linkages between volcanotectonic settings, ore-fluid compositions, and epithermal precious-metal deposits: Society of Economic Geologists Special Publication 10, p. 315–343.
Simmons, S.F., 1995, Magmatic contributions to low-sulfidation epithermal deposits: Magmas, fluids, and ore deposits: Mineralogical Society of Canada Short Course Notes, v. 23, p. 455–477.
Simmons, S.G., and Brown, K.L., 2002, Metallogeny in a modern subduction zone setting, North Island, New Zealand [abs.]: Geological Society of America Abstracts with Program, v. 34, no. 6, p. A-13.
Spell, T.L., and Harrison, T.M., 1993, $^{40}Ar/^{39}Ar$ of post-Valles caldera rhyolites, Jemez volcanic field, New Mexico: Journal of Geophysical Research, v. 98, p. 8031–8051.
Spell, T.L., McDougall, I., and Doulgeris, A.P., 1996, Cerro Toledo Rhyolite, Jemez volcanic field, New Mexico: $^{40}Ar/^{39}Ar$ geochronology of eruptions between two caldera-forming events: Geological Society of America Bulletin, v. 108, p. 1549–1566.
Steiger, R.H., and Jager, E., 1977, Subcommission of geochronology: Conventions on the use of decay constants in geo- and cosmochronology: Earth and Planetary Science Letters, v. 36, p. 359–362.
Steven, T.A., Mehnert, H.H., and Obradovich, J.D., 1967, Age of volcanic activity in the San Juan Mountains, Colorado: U.S. Geological Survey Professional Paper 575-D, p. 47–55.
Stewart, J.H., and Carlson, J.E., 1976, Cenozoic rocks of Nevada: Nevada Bureau of Mines and Geology Map 52, scale 1:1,000,000.
Taylor, H.P., Jr., 1973, $^{18}O/^{16}O$ evidence for meteoric-hydrothermal alteration and ore deposition in the Tonopah, Comstock Lode, and Goldfield mining districts, Nevada: ECONOMIC GEOLOGY, v. 68, p. 747–764.
Theodore, T.G., Armstrong, A.K., Harris, A.G., Stevens, C.G., and Tosdal, R.M., 1998, Geology of the northern terminus of the Carlin trend, Nevada—links between crustal shortening during the Late Paleozoic Humboldt orogeny and northeast-striking faults: U.S. Geological Survey Open-File Report 98-338, p. 69–105.
Vikre, P.G., 1985, Precious metal vein systems in the National district, Humboldt County, Nevada: ECONOMIC GEOLOGY, v. 80, p. 360–393.
——1989, Fluid-mineral relations in the Comstock lode: ECONOMIC GEOLOGY, v. 84, p. 1574–1613.
Wallace, A.R., 1993, Geologic map of the Snowstorm Mountains and vicinity, Elko and Humboldt counties, Nevada: U.S. Geological Survey Miscellaneous Investigations Series Map I-2394, scale 1:50,000.
——2003, Geology of the Ivanhoe Hg-Au district, northern Nevada: Influence of Miocene volcanism, lakes, and active faulting on epithermal mineralization: ECONOMIC GEOLOGY, v. 98, p. 409–424.
Wallace, A.R., and McKee, E.H., 1994, Implications of Eocene through Miocene ages for volcanic rocks, Snowstorm Mountains and vicinity, northern Nevada: U.S. Geological Survey Bulletin 2081, p. 13–18.
Wallace, A.R., McKee, E.H., Zoback, M.L., and Zimmermann, R.A., 1990, New ages for volcanic rocks, western Elko county, Nevada: Isochron/West, no. 55, p. 3–5.
Wendt, I., and Carl, C., 1991, The statistical distribution of the mean squared weighted deviation: Chemical Geology, v. 86, p. 275–285.

York, D., 1969, Least squares fitting of a straight line with correlated errors: Earth and Planetary Science Letters, v. 5, p. 320–324.
Young, H.D., 1962, Statistical treatment of experimental data: New York, McGraw Hill, 172 p.
Zoback, M.L., and Thompson, G.A., 1978, Basin and Range rifting in northern Nevada: Clues from a mid-Miocene rift and its subsequent offsets: Geology, v. 6, p. 111–116.
Zoback, M.L., McKee, E.H., Blakely, R.J., and Thompson, G.A., 1994, The northern Nevada rift: Regional tectono-magmatic relations and middle Miocene stress direction: Geological Society of America Bulletin, v. 106, p. 371–382.

APPENDIX 1

Sample Descriptions

MI-S-1 (Tbg): The basaltic andesite is medium to coarsely crystalline with a bimodal size distribution of tabular plagioclase and an intersertal texture. Larger subhedral grains of plagioclase (1.0–3.0 mm, 5 vol %) exhibit oscillatory and normal zoning with compositions ranging from labradorite to oligoclase; some contain minor inclusions of pyroxene and glass. Smaller laths of oligoclase (0.1–0.3 mm, 50–60 vol %) are subophitically enclosed by pyroxene or occur within interstitial, brown glass. Mafic minerals include rounded grains of iddingsitized olivine (0.1–0.5 mm, 2–3 vol %) commonly enclosed in pyroxene. Hypersthene is present in scattered subhedral grains (0.5 mm, 2–3 vol %). Calcic clinopyroxene (augite; 0.5–5 mm, 15–20 vol %) is subophitic about plagioclase and locally shows exsolution of orthopyroxene. The groundmass (5–10 vol %) is composed of interstitial brown glass with microlites of plagioclase and a trace of apatite. Opaque minerals include elongate ilmenite (0.3–0.6 mm, 2–3 vol %) and traces of primary pyrrhotite and chalcopyrite. Mafic minerals and the groundmass have been variably replaced by chlorite. Plagioclase contains a trace of clay (montmorillonite) and calcite along fractures.

MKK-PG-29 (Tbg): This sample is a coarse-grained basalt with laths of randomly oriented oligoclase (0.1–0.3 mm, 50–55 vol %) and clinopyroxene (augite; 0.3–0.5 mm, 15–20 vol %) subophitic about plagioclase. A few larger grains of plagioclase (0.5–2 mm, 2–3 vol %) exhibit oscillatory and normal zoning from labradorite to oligoclase, some of these grains contain spongy cores with abundant inclusions of glass and minor pyroxene. Mafic minerals include augite (0.2–1.0 mm, 15–20 vol %), hypersthene (0.5 mm, 1 vol %), and rounded olivine (0.1–0.3 mm, 1–2 vol %). Opaques include subhedral, elongate ilmenite (0.01–0.1 mm, 1–2 vol %), locally subophitic about plagioclase, and a trace of pyrrhotite and chalcopyrite. The intersertal texture contains interstitial brown glass. Chlorite has variably replaced olivine, hypersthene, and glass. A few fractures contain minor iron oxides and chlorite, and plagioclase locally contains clay-coated fractures.

MI-S-17 (Tepu): This sample is a crystal-rich, vitric rhyolite tuff that contains subhedral sanidine (0.5–1 mm, 8–10 vol %), subangular to subround plagioclase (0.2–0.3 and 1.0–2.0 mm, 3–5 vol %), and subround quartz (0.2–0.2 mm, 1–2 vol %) in a devitrified, felsitic matrix. Lithic fragments include lapilli of andesite or dacite (1–2 mm, 2–3 vol %) and pumice (1–2 mm, 2–3 vol %). The matrix is devitrified, and plagioclase and pumice are partially replaced by kaolinite and smectite. A few sanidines show weak mottling. The sample is cut by two veinlets containing inclusion-rich quartz (0.1–0.3 mm, ~1 vol %), microcrystalline quartz, and zoned rhombs of adularia (0.05–0.1 mm, <1 vol %).

MI-S-61 (Trf): This sample is a flow-banded, porphyritic rhyolite with euhedral to angular, fractured phenocrysts of sanidine (0.5–3.0 mm, 3–4 vol %), rounded albite (1.0–3.0 mm, <1 vol %), and angular to subhedral quartz (0.5 mm, 1 vol %), opaques (0.1 mm, 1 vol %), and a trace of zircon in a glassy matrix exhibiting spherulitic and axiolitic devitrification. Goethite and hematite are present along fractures replacing plagioclase (mafic inclusions) and opaques.

MI-S-70 (Trdf): This sample is a weakly welded rhyodacitic tuff with phenocrysts of anhedral, fractured sanidine (0.2–1.0 mm, 10–15 vol %), minor albite (0.5 mm, 1 vol %), rounded pyroxene (0.25 mm, 1–2 vol %), zircon (0.05–0.1 mm, trace), opaque minerals including hematite (0.05 mm, 1–2 vol %), leucoxene (0.05–0.1 mm, 1 vol %), magnetite (0.05 mm, trace), and light brown glass shards (0.05–0.5 mm, 30–40 vol %). Lithic fragments include pumice fragments (0.5–1.0 mm, 1–2 vol %), clumps or glomerocrysts of rounded fragments of chalcedony with euhedral zircons, pyroxenes altered to iron oxides, and albite (0.5–1.0 mm, 2 vol %), and mafic lapilli (0.5 mm, 1 vol %). The glassy matrix is fresh.

MI-5-4 (Colorado Grande vein, outer bands, spiral 4, 5,250 level, 462-ft S): This sample is from the outer margin of a crustiform portion of the Colorado Grande vein. Bands are variably composed of bladed and patchy calcite, mosaic and comb quartz, rhombohedral, bladed, and anhedral adularia with minor interstitial fluorite (grains are 0.01–1.0 mm). Selenides, electrum, and pyrite (0.01–0.2 mm) are typically associated with mosaic quartz and adularia. A late band is brecciated with calcite filling the matrix around milled fragments of quartz and adularia.

MI-5-3 (Colorado Grande vein, inner bands, spiral 4, 5,250 level, 462-ft S): This sample is from inner bands of a crustiform portion of the Colorado Grande vein. Bands are variably composed of bladed and patchy calcite, mosaic and comb quartz, rhombohedral, bladed and anhedral adularia with minor interstitial fluorite (grains are 0.01–1.0 mm). Silver selenides, electrum, and pyrite (0.01–0.2 mm) are most commonly associated with mosaic quartz and adularia. Minor replacement of bladed calcite by silica is evident in late bands.

MI-S-7 (Eastern Star vein): This sample is from a banded vein at the Eastern Star prospect. Colloform bands range in thickness from 0.1 to 1.0 mm in width and contain variable amounts of quartz and adularia. Minor bladed calcite has been replaced by quartz. Quartz displays a variety of textures including jigsaw, flamboyant, moss, and comb textures and is generally micro- to cryptocrystalline. Adularia is rhombic to anhedral, with larger rhombs (to 0.05 mm) forming in vugs. Silver selenides and electrum (0.01–0.01 mm) are commonly associated with jigsaw quartz and adularia.

APPENDIX 2

Sample Preparation, Analytical Procedures, and Data Reduction

Sample preparation and analytical procedures

Samples used for $^{40}Ar/^{39}Ar$ analysis were crushed and sieved to between 100 and 700 μm and rinsed with dilute HCl to remove calcite. Heavy liquid, magnetic separation, and handpicking techniques were used to produce mineral separates which were rinsed in dilute HF and cleaned in distilled water and acetone. All mineral separate samples were >99 percent pure based on visual examination.

$^{40}Ar/^{39}Ar$ analyses were carried out by the Nevada Isotope Geochronology Laboratory at the University of Nevada, Las Vegas. Samples were packaged with fluence monitors (ANU 92-176, Fish Canyon Tuff sanidine) and synthetic K glass and optical-grade CaF_2 to monitor neutron-induced argon interferences from K and Ca. Samples were irradiated for 14 h in the 1-MW TRIGA-type reactor at the Nuclear Science Center at Texas A&M University. Measured $(^{40}Ar/^{39}Ar)_K$ values were 1.38 (±0.30) × 10^{-2}. Calcium correction factors were $(^{37}Ar/^{39}Ar)$ Ca = 2.78 (±0.20) × 10^{-4} and $(^{39}Ar/^{37}Ar)$ Ca = 6.82 (±0.11) × 10^{-4}. To correct for variations in neutron flux, an error in J of 0.5 percent was used in age calculations. Step heating was carried out in a vacuum resistance furnace. Laser fusion analyses of individual grains were carried out with a CO_2 laser. Argon analyses were performed on a MAP 215-50 mass spectrometer.

Data reduction, statistical analysis, and general interpretation

Reduction of data and age calculations were carried out with software written by Ludwig (1992). Ages for samples were calculated using an assigned age of 27.9 Ma for the Fish Canyon Tuff sanidine flux monitor (Steven et al., 1967; Cebula et al., 1986). Calculated total gas (integrated) ages of step-heated samples are based on weighting by the amount of ^{39}Ar released from each step (Table 1). For step-heated samples, a plateau age is calculated from three or more contiguous steps in which a significant percentage of the gas was released (≥50%), and the contiguous steps or ages overlap at the 2σ confidence level. Inverse isochron analysis of apparent age spectra was used to test for the presence of excess argon using methods described by Deino and Potts (1990) and Spell and Harrison (1993), using the York (1969) routine. The mean square of weighted deviates (MSWD) criteria of Wendt and Carl (1991) were used to assess the reliability of isochrons. An MSWD of less than 2.0 for 10 data points is considered acceptable. If excess argon is indicated, a plateau age is considered a maximum estimate of the age of the sample.

For several sanidine-bearing rhyolites (MI-S-61 and MI-S-70), laser fusion of 10 individual crystals from each sample produced multiple ages. This method provides a means of identifying mixed populations of juvenile, altered and/or xenocrystic sanidines (Spell et al., 1996), a common characteristic of tuffs. Following calculation of sample means and population standard deviations, outliers (samples greater than 2σ from the mean) were removed. A weighted mean age was determined for the revised data set for each sample using methods described by Young (1962). The calculated age using these criteria is considered to reflect the age of juvenile material. Isochron ages were also calculated, using methodology described for step-heated samples. In general, if data display a sufficient spread in radiogenic yield, the resultant isochron is usually reliable and gives the preferred age of the unit (Spell et al., 1996).

APPENDIX 3

Analytical Data

MKK-PG-29, plagioclase, 16.76 mg, J = 0.0009660 ± 0.5%
4 amu discrimination = 1.01545 ± 0.35%, $^{40/39}$K = 0.01207 ± 83.0%, $^{36/37}$Ca = 0.0002723 ± 4.28%, $^{39/37}$Ca = 0.0006968 ± 1.73%

Step	T (°C)	t (min)	^{36}Ar	^{37}Ar	^{38}Ar	^{39}Ar	^{40}Ar	%^{40}Ar*	%^{39}Ar rlsd	Ca/K	^{40}Ar*/^{39}Ar$_K$	Age (Ma)	1s.d.
1	700	12	5.59	98.39	1.36	11.08	1757.69	8.30	16.47	33.18	13.182	22.83	0.98
2	800	12	0.85	109.74	0.31	11.39	344.65	34.20	16.93	36.01	9.890	17.15	0.23
3	900	12	0.50	142.90	0.27	13.63	255.11	54.00	20.26	39.22	9.466	16.42	0.21
4	1,000	12	0.42	127.89	0.22	11.86	213.19	56.20	17.63	40.35	9.299	16.13	0.19
5	1,080	12	0.23	76.87	0.13	7.53	125.93	65.60	11.19	38.20	9.277	16.10	0.19
6	1,150	12	0.22	51.98	0.10	5.12	100.52	75.30	7.61	37.97	9.131	15.84	0.16
7	1,225	12	0.25	20.69	0.09	3.21	99.95	53.40	4.77	24.00	10.190	17.67	0.25
8	1,300	12	0.25	14.02	0.07	1.59	87.25	36.90	2.36	32.92	11.252	19.50	0.36
9	1,400	12	0.29	19.78	0.09	1.86	98.34	39.50	2.76	39.80	9.226	16.01	0.88
						Cumulative %^{39}Ar rlsd =			100.00		Total gas age =	17.59	0.17
											Plateau age =	16.08	0.18
											(steps 3–6)		

MI-S-1, plagioclase, 10.93 mg, J = 0.001448 ± 0.5%
4 amu discrimination = 1.01809 ± 0.17%, $^{40/39}$K = 0.0233 ± 117.44%, $^{36/37}$Ca = 0.0002871 ± 1.76%, $^{39/37}$Ca = 0.0006773 ± 0.29%

Step	T (°C)	t (min)	^{36}Ar	^{37}Ar	^{38}Ar	^{39}Ar	^{40}Ar	%^{40}Ar*	%^{39}Ar rlsd	Ca/K	^{40}Ar*/^{39}Ar$_K$	Age (Ma)	1s.d.
1	600	12	0.95	11.75	0.19	0.78	307.74	11.40	1.72	51.47	45.391	114.84	3.97
2	700	12	0.14	51.81	0.06	3.26	58.53	48.90	7.21	54.35	7.960	20.67	0.53
3	800	12	0.42	126.93	0.18	7.38	158.90	35.5	16.33	58.85	7.451	19.36	0.46
4	900	12	0.40	185.57	0.21	10.29	166.73	46.9	22.79	61.70	7.410	19.25	0.52
5	975	12	0.15	120.77	0.11	6.58	65.99	74.8	14.57	62.81	6.053	15.74	0.17
6	1,050	12	0.09	50.11	0.05	2.86	37.31	75.2	6.33	59.93	6.295	16.37	0.30
7	1,125	12	0.10	43.73	0.05	2.41	37.28	61.3	5.33	62.15	6.040	15.71	0.67
8	1,200	12	0.15	138.16	0.11	7.03	68.66	78.8	15.55	67.41	6.261	16.28	0.46
9	1,275	12	0.12	37.69	0.05	2.04	40.80	42.9	4.51	63.31	5.769	15.01	0.72
10	1,400	12	0.18	43.71	0.06	2.56	63.71	42.6	5.66	58.44	6.640	17.26	0.80
						Cumulative %^{39}Ar rlsd =			100.00		Total gas age =	19.37	0.26
											Plateau age =	15.91	0.26
											(steps 5–10)		

MI-S-17, sanidine, 9.98 mg, J = 0.001551 ± 0.5%
4 amu discrimination = 1.01917 ± 0.28%, $^{40/39}$K = 0.02282 ± 136.0%, $^{36/37}$Ca = 0.0002897 ± 4.07%, $^{39/37}$Ca = 0.0006991 ± 6.99%

Step	T (°C)	t (min)	^{36}Ar	^{37}Ar	^{38}Ar	^{39}Ar	^{40}Ar	%^{40}Ar*	%^{39}Ar rlsd	Ca/K	^{40}Ar*/^{39}Ar$_K$	Age (Ma)	1s.d.
1	575	12	12.53	0.15	3.15	51.24	4065.26	10.70	1.40	0.02	8.467	23.54	0.65
2	630	12	3.93	0.12	1.83	81.02	1637.60	30.80	2.22	0.01	6.179	17.21	0.21
3	705	12	2.91	0.15	2.50	145.63	1680.94	50.40	3.99	0.01	5.766	16.06	0.15
4	780	12	1.95	0.12	3.12	213.38	1772.93	68.80	5.84	0.00	5.670	15.80	0.14
5	855	12	1.55	0.12	3.92	279.94	2026.70	78.40	7.66	0.00	5.643	15.72	0.13
6	930	12	1.24	0.13	4.09	298.69	2028.14	83.00	8.18	0.00	5.599	15.60	0.13
7	1,005	12	1.66	0.13	3.98	284.79	2080.87	77.50	7.80	0.00	5.626	15.67	0.13
8	1,080	12	1.41	0.13	3.59	256.09	1854.73	78.60	7.01	0.00	5.651	15.74	0.13
9	1,155	12	2.34	0.13	3.39	227.13	1962.65	66.00	6.22	0.00	5.662	15.78	0.14
10	1,235	12	3.27	0.16	3.80	241.37	2314.99	59.40	6.61	0.00	5.665	15.78	0.14
11	1,310	12	11.14	0.25	14.58	961.06	8662.84	62.60	26.31	0.00	5.655	15.75	0.14
12	1,365	12	5.29	0.13	8.66	594.55	4920.71	68.90	16.28	0.00	5.696	15.87	0.14
13	1,400	12	0.79	0.06	0.39	17.54	331.12	33.00	0.48	0.02	5.808	16.18	0.28
						Cumulative %^{39}Ar rlsd =			100.00		Total gas age =	15.91	0.11
											Plateau age =	15.75	0.11
											(steps 4–13)		

APPENDIX 3 *(Cont.)*

MI-S-7, adularia, 5.48 mg, J = 0.0009635 ± 0.5%
4 amu discrimination = 1.01545 ± 0.35%, $^{40/39}$K = 0.01207 ± 83.0%, $^{36/37}$Ca = 0.0002723 ± 4.28%, $^{39/37}$Ca = 0.0006968 ± 1.73%

Step	T (°C)	t (min)	^{36}Ar	^{37}Ar	^{38}Ar	^{39}Ar	^{40}Ar	%^{40}Ar*	%^{39}Ar rlsd	Ca/K	^{40}Ar*/^{39}Ar$_K$	Age (Ma)	1s.d.
1	650	12	5.26	0.06	1.43	35.94	1828.54	16.50	3.46	0.01	8.343	14.44	0.32
2	725	12	1.41	0.06	0.91	49.03	832.01	51.80	4.72	0.00	8.610	14.90	0.13
3	800	12	0.93	0.06	1.17	78.13	954.63	73.10	7.52	0.00	8.781	15.20	0.12
4	880	12	0.62	0.07	1.52	107.43	1125.62	85.50	10.35	0.00	8.834	15.29	0.11
5	960	12	0.50	0.06	1.47	104.88	1072.06	88.00	10.10	0.00	8.852	15.32	0.11
6	1,015	12	0.50	0.07	1.11	78.24	835.71	84.70	7.53	0.00	8.849	15.32	0.11
7	1,070	12	0.57	0.07	1.01	70.27	789.65	80.00	6.77	0.00	8.876	15.36	0.11
8	1,150	12	0.97	0.08	1.43	95.77	1131.49	77.70	9.22	0.00	8.893	15.39	0.11
9	1,220	12	1.63	0.09	2.21	145.84	1777.77	74.60	14.04	0.00	8.921	15.44	0.12
10	1,270	12	1.69	0.08	2.31	152.25	1846.29	75.00	14.66	0.00	8.933	15.46	0.12
11	1,320	12	1.18	0.08	1.54	100.71	1246.98	74.90	9.70	0.00	9.010	15.59	0.12
12	1,360	12	0.45	0.07	0.30	17.74	292.61	67.70	1.71	0.01	9.072	15.70	0.15
13	1,400	12	0.34	0.09	0.09	2.19	115.20	21.40	0.21	0.15	5.860	10.16	0.75
						Cumulative %^{39}Ar rlsd =			100.00	Total gas age =		15.33	0.10
										Plateau age =		15.39	0.10
										(steps 4–11)			

MI-5-3, adularia, 5.74 mg, J = 0.001211 ± 0.5%
4 amu discrimination = 1.01691 ± 0.25%, $^{40/39}$K = 1.0E-10 ± 0.00%, $^{36/37}$Ca = 0.0002844 ± 1.16%, $^{39/37}$Ca = 0.0006999 ± 2.90%

Step	T (°C)	t (min)	^{36}Ar	^{37}Ar	^{38}Ar	^{39}Ar	^{40}Ar	%^{40}Ar*	%^{39}Ar rlsd	Ca/K	^{40}Ar*/^{39}Ar$_K$	Age (Ma)	1s.d.
1	600	12	2.62	0.43	0.76	20.31	886.80	15.10	1.15	0.08	6.244	13.59	0.27
2	700	12	1.12	1.39	1.12	71.63	826.06	64.60	4.06	0.07	7.038	15.31	0.11
3	800	12	0.54	0.51	2.46	179.40	1412.46	92.10	10.18	0.01	7.031	15.30	0.09
4	875	12	0.37	0.43	2.99	221.70	1660.13	96.50	12.58	0.01	7.040	15.32	0.09
5	965	12	0.42	0.36	4.02	303.26	2249.51	97.40	17.21	0.00	7.054	15.35	0.09
6	1,040	12	0.43	0.26	3.42	257.45	1937.25	96.70	14.61	0.00	7.075	15.39	0.09
7	1,090	12	0.39	0.15	2.25	165.12	1281.80	95.90	9.37	0.00	7.114	15.48	0.09
8	1,160	12	0.47	0.13	1.58	114.30	948.77	92.40	6.48	0.00	7.128	15.51	0.09
9	1,225	12	1.00	0.18	2.14	150.46	1372.29	83.10	8.54	0.00	7.217	15.70	0.10
10	1,290	12	2.13	0.14	2.87	190.78	1992.52	71.40	10.82	0.00	7.222	15.71	0.10
11	1,325	12	1.00	0.09	1.24	80.64	858.76	72.00	4.58	0.00	7.068	15.38	0.10
12	1,400	12	0.41	0.09	0.18	7.56	172.07	84.40	0.43	0.04	7.703	16.75	0.14
						Cumulative %^{39}Ar rlsd =			100.00	Total gas age =		15.42	0.09
										Plateau age =		15.38	0.08
										(steps 2–8)			

MI-5-4, adularia, 5.99 mg, J = 0.001211 ± 0.5%
4 amu discrimination = 1.01691 ± 0.25%, $^{40/39}$K = 1.0E-10 ± 0.00%, $^{36/37}$Ca = 0.0002844 ± 1.16%, $^{39/37}$Ca = 0.0006999 ± 2.90%

Step	T (°C)	t (min)	^{36}Ar	^{37}Ar	^{38}Ar	^{39}Ar	^{40}Ar	%^{40}Ar*	%^{39}Ar rlsd	Ca/K	^{40}Ar*/^{39}Ar$_K$	Age (Ma)	1s.d.
1	600	12	4.42	0.06	1.04	16.62	1409.64	9.30	0.94	0.01	7.634	16.60	0.49
2	700	12	1.31	0.07	0.81	43.27	682.66	47.60	2.45	0.01	7.004	15.24	0.12
3	800	12	0.81	0.08	1.55	106.64	983.19	80.20	6.05	0.00	7.059	15.36	0.10
4	880	12	0.41	0.08	2.06	151.80	1176.37	93.70	8.61	0.00	6.994	15.22	0.09
5	960	12	0.41	0.07	2.80	207.31	1569.53	96.40	11.76	0.00	7.041	15.32	0.09
6	1,015	12	0.40	0.07	2.32	174.06	1335.66	95.90	9.87	0.00	7.046	15.33	0.09
7	1,070	12	0.43	0.07	2.16	160.04	1245.17	94.80	9.08	0.00	7.040	15.32	0.09
8	1,150	12	0.62	0.08	2.42	175.21	1409.76	91.70	9.94	0.00	7.037	15.31	0.09
9	1,220	12	1.26	0.11	2.53	176.76	1602.50	80.60	10.02	0.00	7.017	15.27	0.10
10	1,280	12	3.37	0.10	4.40	288.15	3004.26	69.00	16.34	0.00	7.056	15.35	0.10
11	1,320	12	2.19	0.08	3.50	239.92	2329.39	76.20	13.60	0.00	7.101	15.45	0.10
12	1,400	12	0.52	0.07	0.39	23.75	318.89	90.30	1.35	0.01	7.321	15.92	0.11
						Cumulative %^{39}Ar rlsd =			100.00	Total gas age =		15.35	0.08
										Plateau age =		15.30	0.08
										(steps 2–10)			

APPENDIX 3 *(Cont.)*

MI-S-61, sanidine, J = 0.001449 ± 0.5%
4 amu discrimination = 1.01898 ± 0.23%, $^{40/39}$K = 0.0233 ± 117.44%, $^{36/37}$Ca = 0.0002871 ± 1.76%, $^{39/37}$Ca = 0.0006773 ± 0.29%

Crystal	T (C)	t (min.)	^{36}Ar	^{37}Ar	^{38}Ar	^{39}Ar	^{40}Ar	%^{40}Ar*	Ca/K	^{40}Ar*/^{39}Ar$_K$	Age (Ma)	1s.d.
1	1600	6	0.32	4.96	1.98	144.91	964.05	90.40	0.12	6.027	15.69	0.12
2	1600	6	0.21	4.28	1.54	116.53	759.58	92.30	0.13	6.027	15.69	0.12
3	1600	6	0.12	2.13	1.06	80.63	517.66	93.80	0.10	6.018	15.66	0.12
4	1600	6	0.11	2.46	0.94	71.12	453.46	93.80	0.12	5.981	15.57	0.12
5	1600	6	0.19	2.53	1.14	85.78	567.50	90.60	0.11	6.001	15.62	0.12
6	1600	6	0.12	3.59	1.19	88.91	567.76	94.20	0.14	6.026	15.68	0.12
7	1600	6	0.12	2.73	0.91	68.15	442.41	93.00	0.14	6.040	15.72	0.12
8	1600	6	0.08	2.08	0.66	50.05	322.10	93.40	0.15	6.004	15.63	0.12
9	1600	6	0.05	2.70	1.12	84.39	516.01	97.70	0.12	5.981	15.57	0.12
10	1600	6	0.08	2.20	0.89	67.41	428.66	94.80	0.12	6.031	15.70	0.12
										Mean ± s.d. =	15.65	0.05
										wtd mean =	15.65	0.08

MI-S-70, sanidine, J = 0.0015535 ± 0.5%
4 amu discrimination = 1.02136 ± 0.32%, $^{40/39}$K = 0.00 ± 0.0002%, $^{36/37}$Ca = 0.000282 ± 1.51%, $^{39/37}$Ca = 0.000677 ± 0.81%

Crystal	T (C)	t (min.)	^{36}Ar	^{37}Ar	^{38}Ar	^{39}Ar	^{40}Ar	%^{40}Ar*	Ca/K	^{40}Ar*/^{39}Ar$_K$	Age (Ma)	1s.d.
1	1600	6	0.12	3.62	0.97	71.91	418.66	92.30	0.17	5.375	15.00	0.16
2	1600	6	0.07	2.92	1.10	82.88	473.03	96.10	0.12	5.486	15.31	0.11
3	1600	6	0.08	1.93	0.58	42.69	261.47	91.50	0.15	5.586	15.59	0.12
4	1600	6	0.04	1.23	0.31	24.71	144.94	94.40	0.17	5.487	15.31	0.15
5	1600	6	0.31	4.92	1.28	91.76	599.74	85.90	0.18	5.628	15.71	0.11
6	1600	6	0.05	3.65	1.11	82.95	466.33	97.60	0.15	5.495	15.34	0.10
7	1600	6	0.03	1.44	0.35	26.90	154.06	98.00	0.18	5.575	15.56	0.17
8	1600	6	0.03	1.92	0.59	43.76	244.44	98.50	0.15	5.491	15.32	0.11
9	1600	6	0.07	3.75	0.93	70.86	403.34	96.20	0.18	5.478	15.29	0.11
10	1600	6	0.71	4.76	1.09	72.87	627.71	68.10	0.22	5.880	16.40	0.13
										Mean ± s.d. =	15.48	0.36
										wtd mean =	15.39	0.08

Notes: Isotope beams in mV (^{36}Ar through ^{40}Ar are measured intensities, corrected for decay in age calculations), rlsd = released, error in age includes 0.5% J error; all errors 1 σ